COMPOSITIONAL CHANGES OCCURRING IN ALUMINO-SILICATE REFRACTORIES EXHIBITING INCREASED STRENGTH AT ELEVATED TEMPERATURES

A THESIS

Presented to

the Faculty of the Graduate Division

by

Russell Guy Smith

In Partial Fulfillment

of the Requirements for the Degree

Master of Science in Ceramic Engineering

Georgia Institute of Technology

June, 1968

COMPOSITIONAL CHANGES OCCURRING IN ALUMINO-SILICATE REFRACTORIES EXHIBITING INCREASED STRENGTH AT ELEVATED TEMPERATURES

Approved:

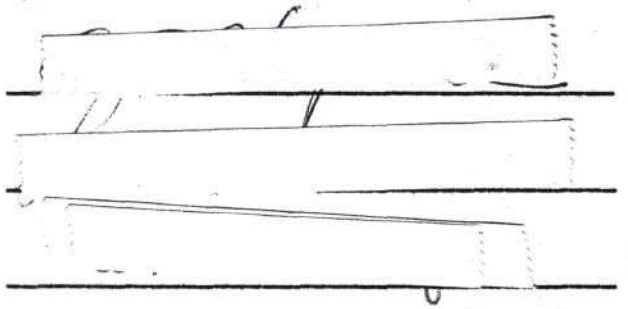

Date Approved by Chairman: May 22, 1968

In presenting the dissertation as a partial fulfillment of the requirements for an advanced degree from the Georgia Institute of Technology, I agree that the Library of the Institute shall make it available for inspection and circulation in accordance with its regulations governing materials of this type. I agree that permission to copy from, or to publish from, this dissertation may be granted by the professor under whose direction it was written, or, in his absence, by the Dean of the Graduate Division when such copying or publication is solely for scholarly purposes and does not involve potential financial gain. It is understood that any copying from, or publication of, this dissertation which involves potential financial gain will not be allowed without written permission.

3/17/65
b

ACKNOWLEDGMENTS

The author wishes to thank the Edward Orton Jr. Ceramic Foundation and the Georgia Institute of Technology for funds which made this investigation possible.

The author also wishes to express his appreciation to Dr. A. T. Chapman for his interest and willingness to assist at any time, and to Dr. W. E. Moody and Dr. Lane Mitchell for their interest and suggestions while serving on the reading committee.

The author wishes to thank the Babcock and Wilcox Co. for the raw materials used in this investigation.

The encouragement and assistance of my wife, Priscilla, is deeply appreciated.

TABLE OF CONTENTS

TABLE OF CONTENTS (Continued)

LIST OF TABLES

LIST OF TABLES (Continued)

LIST OF FIGURES

SUMMARY

Multiphase alumino-silicate refractories increase in mechanical strength from room temperature to approximately 2000°F. Although no explanation for this behavior has been universally accepted, the most logical causes are releasing of induced stresses; closure of cooling cracks and fissures; increased bonding between phases; and increased viscosity of the liquid phase at constant temperature. The purpose of this work was to investigate compositional changes occurring in two alumino-silicate refractories at elevated temperatures and to correlate this change with the observed increased strength.

Compositional changes from room temperature to 2800°F of a high alumina and a mullite firebrick refractory were studied by quantitative x-ray diffraction using the internal standard technique. The specimens were heated for three hours at 1800, 2000, 2300, 2600, and 2800°F. The per cent crystalline phases in quenched samples were determined from standard calibration curves and the per cent noncrystalline phase by difference. Evidence of compositional changes of the mullite was obtained from lattice parameter variations. Strain measurements of both refractories showed the alumina to be in tension at all temperatures.

The results of this study indicate strength increases depend on both composition and temperature changes. Between room temperature and 1800°F the increased strength in both refractories resulted from the closure of cracks, increased cohesive forces between particles, and compositional changes in the glassy phase. Above 1800°F in the mullite

refractory the amount of glassy phase decreased, cristobalite was formed, and the Al_2O_3 content of the mullite phase decreased during heating. In the high alumina refractory in this same temperature range, a portion of the crystalline Al_2O_3 entered the glassy material, and also entered the mullite lattice to increase the Al_2O_3 content of this phase. The influence of these compositional changes on the mechanical strength at 2000°F are described.

CHAPTER I

INTRODUCTION

The phenomenon of increased strength at elevated temperatures of multiphase alumino-silicate refractories has been known for years; yet no universally acceptable explanation exists. The most logical reasons that have been given to date are: (1) increased viscosity of the liquid phase; (2) progressive releasing of induced stresses; (3) healing of cooling cracks and fissures; and (4) bond strength development during heat treatment.

The purpose of this work was to investigate compositional changes of alumino-silicate refractories and what effect they have on increased strength at elevated temperatures. The compositional changes from room temperature to 2800°F were investigated with quantitative x-ray diffraction techniques. From the results of these measurements and previous theories, an explanation of the increased strength at elevated temperatures of alumino-silicate refractories is given.

CHAPTER II

REVIEW OF THE LITERATURE

Investigations to date indicate that increased strength at elevated temperatures is restricted to systems possessing certain characteristics. Studies of these systems have produced various theories to explain this phenomenon. Releasing of stresses, closure of voids, compositional changes, thermal expansion properties, and changes in the properties of the liquid phase all seem to affect the strength of multiphase bodies at elevated temperatures.

Systems Exhibiting Increased Strength at Elevated Temperatures

Since the phenomenon of increased strength at elevated temperatures of ceramic materials was first reported by Hunt and Bradley (1) in 1941, many investigators have tried to determine the causes and to which systems, if any, it is restricted. The major criteria which a system must possess to exhibit this phenomenon are to be a heterogeneous multiphase system, or to be a single phase aggregate of anisotropic crystals.

This phenomenon is most pronounced in systems containing large amounts of free silica. However, this effect is by no means limited to silica refractories. Chrome-magnesite and other basic refractories (2,3), alumina refractories containing up to about 90 per cent alumina, and fireclay materials containing free crystalline silica (4) exhibit this behavior. Fleming (5) has shown that the strength of fused silica

increases with increasing temperature. Fleming believes a possible cause for this is the partial devitrification of fused silica into cristobalite.

Bush and Hummel (6,7) found increased strength at elevated temperatures exists in sintered aggregates of β-eucryptite and magnesium dititanate, both of which are extremely anisotropic crystals.

Strength at Elevated Temperatures

Hunt and Bradley (1) conducted hot modulus of rupture and hot crushing strength tests on fireclay bricks, a 60 per cent alumina diaspore brick, and an insulating fire brick. They reported constant modulus of rupture from room temperature to approximately 1800°F with strength increases in the 1800° to 2000°F range.

Davis and Rigby (8, 9) determined Young's Modulus of eight silica brick compositions and eight alumino-silicate compositions from room temperature to 1000°C, and also the changes in Young's Modulus after cycling to 1100°C. Young's Modulus of the silica brick was approximately three times greater at 1000°C than room temperature. Thermal cycling to 1100°C increased Young's Modulus, the amount depending on the composition. All of the alumino-silicate bricks increased in Young's Modulus at 1000°C, the amount depending on the composition. Cycling the alumino-silicate bricks first increased the room temperature Young's Modulus but decreased the strength after six cycles.

Miller and Davis (10) tested commercial alumina, fireclay, and silica brick refractories from room temperature to 2900°F. They found peaks in the modulus of rupture versus temperature curves at about 2000°F for fireclay bricks, but no peak or increase of any kind in modulus versus

temperature for 99 per cent alumina bricks. They also determined that the modulus of rupture at room temperature, 2000°F, and 2500°F drops approximately in half when porosity goes from 14 per cent to 20 per cent. Finally, they concluded that modulus of rupture versus impurity content falls off in an exponential manner at 2500°F, reaching a value of about 100 p.s.i. for alumina-silica refractories containing 6 per cent auxiliary oxides.

Folk and Bohling (11) found the same characteristic curve as did Miller and Davis for temperature versus modulus of rupture, namely, an essentially constant modulus of rupture value from room temperature to about 1500°F with a peak between 1500°F and 2300°F, with almost complete loss of strength in the neighborhood of 3000°F. The peak became less prominent as the percentage of alumina increased, until it was non-existent at 95 per cent alumina. They also ran a series of modulus of rupture versus temperature tests for various initial firing temperatures. They found the higher firings yielded the highest strengths. All of their samples were broken after a four and one-half hour soak at the breaking temperature.

Present Theories of Increased Strength

The gain in strength of alumino-silica refractories in the temperature range between 1500°F and 2000°F has been studied by several investigators, and almost as many theories have been put forth as to its cause as there have been accounts in the literature reporting this phenomenon. Therefore, a brief review of these theories is in order. It is unlikely that any one theory can account for this phenomenon, and a

combination of these theories, depending on the material, are necessary to explain this behavior.

Induced Stresses

The theory of stress changes, resulting from dissimilar phases possessing different coefficients of thermal expansion, causing increase in strength at elevated temperatures is dealt with at some length in Rigby's publications (8, 9, 12).

Rigby suggested Young's Modulus and strength increases must be caused by some factor introduced by the association of the glass and crystalline phases. Since the thermal expansion properties of glasses are usually higher than those of crystalline materials, on cooling, the crystals would contract less than the glass which surrounds them; and at room temperature the material may be in considerable strain. The glass matrix is in tension and the crystals are in compression. On reheating such a specimen, these internal stresses between glass and crystallites would be progressively released as the glass softens and flows. Rigby believes the creation of internal stresses on cooling and them subsequent disappearance on heating afford a ready explanation for the variation of the modulus of elasticity with temperature, since the ability to resist external stresses becomes greater as randomly distributed stresses disappear.

Fulrath (13) studied internal stresses in alumina-glass systems using x-ray diffraction. Fulrath's results indicate internal stresses on the crystal phase decreased the modulus of rupture. For a model system of single crystal oxide particles in a matrix of glass, the stress configuration on cooling is shown in Figure 1 (13). The validity of this

model implies formation of a strong glass-crystal interface. This glass-crystal model system has both continuous glass and crystal phases since crystal contact would be obtained at the points where the spheres touch, and the glass would be continuous throughout the volume not occupied by the crystals.

In Figure 1 (a) the system is shown for the condition in which glass has the higher thermal expansion coefficient. With the crystal-crystal contacts formed at temperatures where the glass is fluid, cooling introduces tensile forces applied normal to the crystal glass interface. At crystal-crystal contacts a compressive stress is developed. Also, since the glass is contracting at a greater rate, the shear force tangential to the interface requires that the glass be in tension and the crystal in compression.

For the opposite condition in which the crystal's thermal expansion coefficient is greater than that of the glass, the normal force to the glass-crystal interface is compressive; and the tangential force places the glass in compression and the crystal in tension. The crystal-crystal contacts are in tension. This condition is shown in Figure 1 (b).

In actual cases, however, serious deviations from this simple model occur. The crystal particles in ceramic bodies are very seldom if ever spherical. Also, packing of non-spherical particles may not follow the model.

Miller and Davis (10) investigated the modulus of rupture behavior at elevated temperatures of eight commercially available alumina-silica refractories ranging in composition from 96.2 per cent silica to 99 per cent alumina. They found that the strength peak was particularly pro-

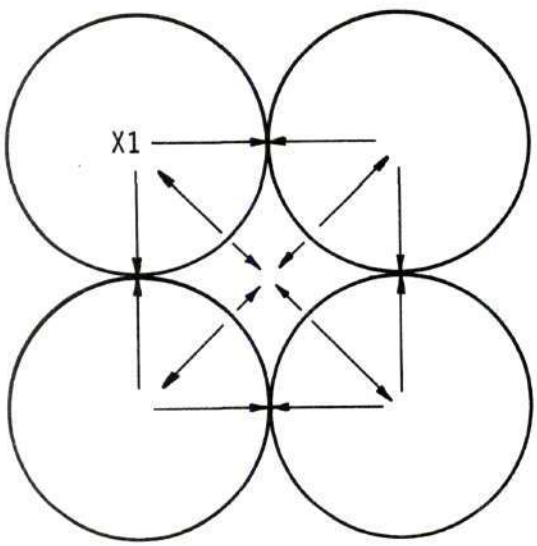

$\alpha_{x1} > \alpha_{g1}$
ON COOLING

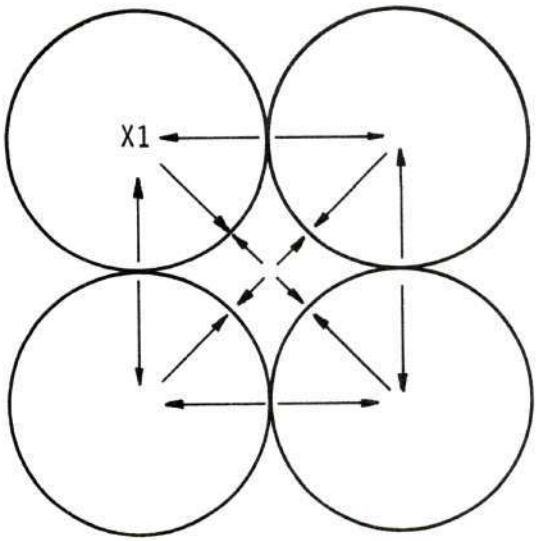

$\alpha_{g1} > \alpha_{x1}$
ON COOLING

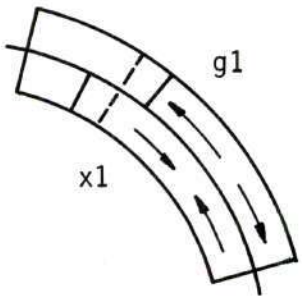

(a)

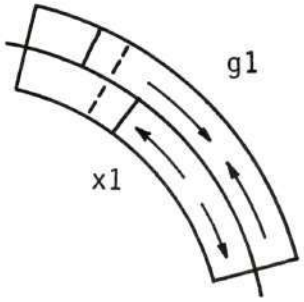

(b)

STRESS ON CRYSTAL

	(a)	(b)
NORMAL TO x1-x1 INTERFACE	COMPRESSION	TENSION
NORMAL TO x1-GLASS INTERFACE	TENSION	COMPRESSION
TANGENTIAL TO x1-GLASS INTERFACE	COMPRESSION	TENSION

Figure 1. Stress Configuration in Model Crystal-Glass Compacts with Open Cubic Packing of Spherical Crystal Particles.

nounced with refractories containing both crystalline and glassy phases. As the amount of glassy phase decreased, the strength peaks became less pronounced until it finally disappeared in the case of the 99 per cent alumina refractory. From their investigation, Miller and Davis (10) concluded, "The gain in strength with increasing temperature and the shape of the strength-temperature curves was controlled by the presence or absence of dissimilar mineral phases possessing different thermal expansions."

Mattyasovsky-Zsolmay (14) found that the mechanical strength of porcelain, in which a glassy phase is the major part, is influenced mainly by stresses set up in the glassy phase. A crystalline material, such as quartz with a high coefficient of thermal expansion, increases the strength of a fired ceramic matrix. He states further, "a system consisting of grains under tensile stress and a matrix under compressive stress is unfavorable for the propagation of Griffith's flaws, as the compressive stresses are barriers in their path."

Healing of Cooling Cracks and Fissures

A relationship between increased strength at elevated temperatures and the filling up of the voids by the phase with the higher thermal expansion has been hypothesized by Roberts (15). "As a result of phases having different thermal expansion characteristics, the contact area between the dissimilar phases is increased on heating and, conversely, is more or less reversibly decreased on cooling." In other words, differential expansion results in reduction of voidage to give an increased contact area or volume to resist the applied stress.

On this hypothesis it follows that the increase in strength that

occurs when a refractory is heated is simply the reversal of physical changes in texture that have taken place during the cooling stage of the initial firing process. When first fired, equilibrium between the relevant crystalline and liquid phases tends to be approached and the crystals tend to become more or less surrounded by the liquid. On cooling, crystals will tend to separate from the liquid once the liquid has solidified, provided that the respective contraction coefficients are sufficiently different. Thus, when cold, the crystalline components are no longer completely surrounded by matrix but are partially or wholly isolated from it by minute voids and fissures.

Chaklader and Roberts (16) were able to observe the closure of cracks in and around the crystals of cristobalite in devitrified silica glass using a cine-camera.

Ault and Ueltz (17) proposed the concept of internal cracking in bodies containing free quartz. They determined modulus of elasticity values up to 800°C for a multiphase ceramic porcelain body by sonic analysis. Modulus of elasticity values for this porcelain body rose gradually from room temperature to 550°C and then rose rapidly up to 600°C. Values of the modulus of elasticity during cooling were almost identical with those obtained during heating. From these results Ault and Ueltz expressed the belief that differential thermal expansion was responsible for this elasticity change and pointed out that it may arise in any of three ways: "(a) from two or more phases having different coefficients of thermal expansion, (b) from an anisotropic phase having different coefficients of linear thermal expansion along its crystallographic axes, and (c) from a phase which inverts to a second phase,

having a volume different from that of the first phase."

Bush and Hummel (6,7) observed an increase in strength at elevated temperatures for single phase sintered aggregates of β-eucryptite ($LiO_2 \cdot Al_2O_3 \cdot 2SiO_2$) and magnesium dititanate. Since both β-eucryptite and magnesium dititanate have extremely anisotropic thermal expansion, internal fractures occur in sintered aggregates of these materials during cooling from the firing temperature because of the stress increase. Upon reheating these internal fractures heal, resulting in increased strength and elastic modulus.

Gillery and Bush (18) have proven the occurrence of these internal voids by the large difference between the macroscopic thermal expansion (measured, for example, by a dial gauge on ceramic bars), and the lattice expansion measured by x-ray back reflections on a powder specimen. From the firing temperature down to about 1000°C, the contraction of the ceramic body and of the crystal lattice is identical; however, upon reaching this temperature and cooling to room temperature, the ceramic body and the lattice behave very differently. The lattice continues to contract at the same rate as before, whereas the contraction rate of the body decreases as the microcracks are formed.

Bond Strength Development During Heat Treatment

Increased bonding between different phases in the refractories during heating can be caused by at least two mechanisms. These mechanisms are cohesive forces from capillary suction and sintering in the presence of a liquid phase. The application of these mechanisms must be limited to systems containing aggregates of solid particles bonded by a liquid phase which coats the particles and forms lenses of liquid

at points of contact. Furthermore, these mechanisms are not entirely independent of one another; however, in this discussion they will be presented separately.

Cohesive Forces from Capillary Suction. The work of Houseman and White (19), Evans and White (20), Allison, Brock and White (21) and Houseman (22) on liquid bonded aggregates reported the increased strength at elevated temperatures characteristic of materials in which there is formation of a liquid phase which freezes during cooling. These investigators indicate the transverse strength of refractories containing a liquid phase can be related to the amount of liquid formed and the amount of fluxing oxides present.

Evans and White (20) considered the initial increase in strength to be associated with the formation of small amounts of a liquid phase in the bond. This phase has a cementing action owing to the high viscosity and to the operation of capillary forces. As the temperature is raised, the increase in the liquid content at first causes the strength to rise; but ultimately, as the liquid content increases, the bond softens, the strength falls, and a peak occurs in the strength-temperature curve. In support of this hypothesis they observed that on the low temperature side of the peak, the test piece failed by shearing without appreciable deformation; whereas, on the high temperature side of the peak, an appreciable degree of plastic flow preceded failure.

Cohesive forces between particles in a liquid bonded aggregate can exist only if the liquid wets the solid. With liquids which wet the solid, cohesion between the particles appear to be due to capillary forces in the liquid phase, which is drawn to points of contact between

the particles to form lenses or necks of liquid. This mechanism is illustrated in Figure 2 (19).

The essential question, however, was whether the magnitude of the cohesive forces is adequate to explain the observed strength of liquid bonded aggregates. Ford and White (2) investigated the strength of basic refractories at high temperatures. Their calculations, based on the assumption that cohesion is due to capillary suctions in the liquid when the bond has melted, give cohesive strengths of the correct order and suggest that the tensile strength of magnesite can be accounted for on this basis. However, Houseman and White's (19) investigation of alumino-silicate refractories showed that calculated cohesive forces are too small. A possible explanation for this discrepancy is, while liquid films were present between certain grains, solid-solid bonding also occurred between others.

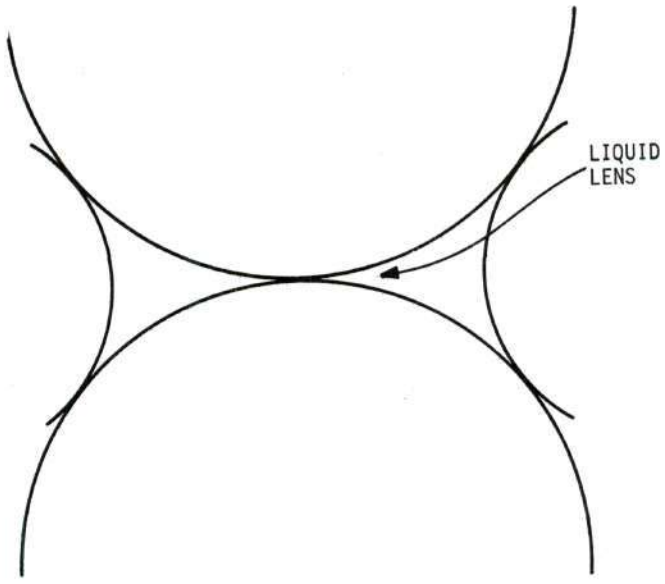

Figure 2. Spherical Particles in Contact Showing Lens of Liquid at Points of Contact.

Sintering in the Presence of a Liquid Phase. The sintering of two particles in the presence of a liquid phase would most likely take place by a solution-precipitation mechanism. Thus, if Figure 2 represents two solid particles in direct contact and having a lens of liquid around the point of contact, capillary theory indicates that the solubility of the solid in the liquid phase will be greater where the liquid is in contact with the convex surfaces of the particles than at the neck between the particles. Hence, solids will tend to dissolve from the surface of the particles and precipitate in the neck and the strength will increase. Ultimately, with increasing temperature and liquid content, the tendency of the liquid phase to penetrate between the particles would increase so that the strength would decrease.

Increased Viscosity of Liquid Phase

Chaklader, Carruthers, and Roberts (23) tested alumino-silicate and silica refractories in torsion at elevated temperatures. They suggested that the "creep" curves obtained might give a first approach to measuring the apparent viscosity of refractories. If the deformation of the refractories at temperatures up to 1100°C is considered to be entirely centered in the glassy phase, these measurements will give the magnitude of the apparent viscosity of the refractory.

The apparent viscosity values obtained for refractory materials were far higher than would be expected from the properties of the glass itself. This high viscosity value appears to suggest that the crystal phases interspersed in the glassy matrix strongly reinforce the strength of the glass. This may occur by two possible mechanisms; the crystals distributed in the glass act as "fillers" and increase the viscosity of

the glass at constant temperature in a manner analogous to the greatly increased viscosity which results when solids are added to a liquid to increase the shear force. Another possible effect is the development of a type of rigid structure within the glass at the interface between the glass and the crystals caused by producing a more ordered structure in the glass at the interface.

Chaklader and Roberts (24) demonstrated the marked increase in rigidity that occurred on heating of silica refractories. They concluded that the higher apparent viscosity of silica refractories at temperatures up to about 1400°C lies in a matrix reinforced by crystals and possibly also in the non-crystalline phase forming the bulk of the matrix. At higher temperatures any tendency of the non-crystalline phase to soften is affected by crystallization, which serves to maintain the already high viscosity.

Davis and Rigby (8) showed that repeated heatings to 1000°C and cooling of silica refractories may decrease the value of Young's Modulus at room temperature, but repeated heatings to 1110°C resulted in an increase in the value of Young's Modulus at room temperature. This is ascribed to solution of silica material into the glass bond at the higher temperature and its precipitation as crystallites on cooling, thus resulting in an increase in the area of the crystal-glass interface with a consequent increase in the rigidity of the glass bond.

The effect on strength of the formation of a second crystalline phase in controlled mullite-glass systems was studied by Studt and Fulrath (25). The glass compositions used ranged from 59 to 81 per cent silica; four to 31 per cent soda and contained either alumina or

boric oxide. By varying the amounts of mullite and glass in hot pressed compacts, they were able to obtain varying amounts of α-cristobalite. From these compacts they found that the α-cristobalite formation first increased the strength and then decreased it when the reaction had reached some equilibrium value.

Reactions in Alumino-Silicate Refractories

The reactions in alumino-silicate refractories which most probably affect high temperature strength are: (1) reactions between the crystalline and glassy phases; (2) compositional changes of the glassy phase causing a change in its physical properties; and (3) compositional changes of the crystalline phases.

Nature of the Non-Crystalline Phase

It is difficult to define the character and amount of glass in refractory materials. The glass that is present in silica and alumino-silicate refractories is probably different from ordinary commercial glass which contains, besides silica, large quantities of soda, potash, lime, and small amounts of alumina. Judging from chemical analysis of various alumino-silicate refractories, one would expect the composition of the glassy phase to differ for the various alumino-silicate refractories. Further changes in composition would take place at high temperatures when some of the crystalline material dissolves in the liquid.

It is usually assumed that the glassy matrix in a refractory contains all the fluxing oxides, with the possible exception of some of the TiO_2 and Fe_2O_3, which are present in the mullite. Also, the glassy matrix contains any excess silica and some alumina. If this is true, it is

impossible to deduce the melting point of the eutectics that would be formed in such a complex system.

Further information concerning the nature of the glassy phase of alumino-silicate and silica refractories is given by Wiechula and Roberts (4) and Chaklader and Roberts (24). Their studies indicate that the "creep" of refractories is largely controlled by the characteristics of the glassy matrix. However, the creep behavior of these refractories is not comparable with viscosities of true glasses.

Chaklader and Roberts (24) state that: "The quantity of true glass in a silica brick, formed by the interaction of the 4-5 per cent of impurities and silica, generally should not exceed about 15 per cent." However, in previous work by Chaklader and Roberts (26) silica brick were shown to contain 36 to 40 per cent of a non-crystalline phase. They assigned the difference of 20-25 per cent to an intermediate transition phase produced when quartz is converted to cristobalite. This phase appears to be remarkably stable, being decomposed only with difficulty below 1600°C.

The viscosity of fused silica held at constant temperature increases rapidly as devitrification occurs (5, 17). The glassy phase of alumino-silicate refractories exhibited an analogous behavior when devitrification occurs.

In seeking an answer to why glass is less deformable when associated with the crystalline components of refractory materials, a parallel problem which exist in clay slips should be considered. Clay slips are much more viscous than water itself. Macey (27) has suggested that the envelopes of water molecules, because of their orientation, possess some

degree of rigidity.

The glassy phase in refractories may be similarly affected, i.e., the intimate association with the crystalline material dispersed through the glass phase may impose some orientation on the glass structure. The degree of orientation will largely depend on the surface area between the crystalline and glassy phases. In order to impose any orientation on the glass phase at all, the crystalline and glassy phase must contain similar atomic linkages such as the Si-O linkage.

Effect of Alumina in Glassy Phase. The type of structure of the glassy phase is not known but is probably of the Frenkel or Stewart type (28). Some of the effects of Al_2O_3 on these structures are known. The addition of alumina to a Frenkel type liquid restores some of the symmetry. Alumina additions change the most polarizable, nonbridging O^{2-} ions into less polarizable, bridging Al-O-Si oxygens. This increase in bridging oxygen increases the strength.

The replacement of silica by alumina in a silicate glass reduces the oxygen ratio and, therefore, increases the strength (28). This decreases the anion/cation ratio and increases the viscosity at constant temperature.

Mullite-Glass Reactions

Studt and Fulrath (25) investigated the reactions in mullite-glass systems. X-ray analysis of these mullite-glass compacts formed by hot pressing indicated the formation of α-cristobalite.

In the mullite-glass compacts studied by Studt and Fulrath definate changes were observed in the mullite structure during the formation of α-cristobalite. Hence it is clear that Al^{3+} and/or Si^{4+} ion

movement was taking place during the reaction.

In Schuller's (29) study of the reaction between mullite and glassy phases in porcelains, he concluded that the silica content of the glass phase is an important factor in its reactivity with mullite. Only in melts high in silica is mullite dissolved during firing.

In support of Studt and Fulrath's (25) conclusion in the reaction of mullite and glass, Majumdar and Welch (30) have determined that long heat treatments of homogeneous mullite solid solutions produced at least a small amount of exsolution. These mullite crystalline solutions precipitate either cristobalite or corundum. The exact nature and degree of exsolution depended on the temperature, the duration of heat treatment, and the composition of the mullite crystals.

Alumina-Glass Reaction

Reaction of alumina and silica have been studied by many investigators. All of these investigations can be grouped into two general categories: (a) studies of the system Al_2O_3 - SiO_2; (b) studies of the Al_2O_3 - SiO_2 - Alkali systems. In both cases the alumina reacts with silica to form mullite; the composition and amount of which depend on many variables, namely, the ratio of alumina and silica free to react, the presence of fluxes, and the crystalline form and structural stability of the alumina and silica. Wahl, Grim, and Graf (31) studied the formation of mullite from mixtures of different varieties of alumina and silica. They showed that the initial form of the alumina and silica has a large influence on mullite formation.

When alkalis are present, they react with the alumina to form a highly viscous liquid and decrease mullitization. However, such oxides

as TiO_2 and Fe_2O_3 increase the amount of mullite formed.

Activation energies for dissolution of corundum as a crystalline phase in pure synthetic silicate melts have been calculated. Interdiffusion is primarily a function of the cations if the concentration gradient is small, and of the anions if the gradient is large. The mechanism of dissolution of corundum as such, however, is still unknown.

Mullite Solid Solutions

It has been firmly established that the composition of mullite can no longer be represented by the simple formula $3Al_2O_3 \cdot 2SiO_2$. The work of Rooksby and Partridge (32) has indicated that there are three varieties of mullite distinguishable by the differences in axial ratios of the unit cell. They are α-mullite made from pure materials corresponding to the formula $3Al_2O_3 \cdot 2SiO_2$ and containing 28.2 per cent SiO_2, 71.8 per cent Al_2O_3; β-mullite contain excess alumina in solution; and γ-mullite contain small proportions of ferric oxide and/or titania in solution. β-mullite can contain as high as 78 per cent alumina, although there is a progressive change in the lattice from the α to the β variety as the alumina content rises above 72 per cent.

Durovic (33) determined the crystal structure of mullite having a chemical composition $1.71\ Al_2O_3 \cdot SiO_2$. He hypothesized that all mullite will exhibit a similar structure, but with a degree of substitution corresponding to their chemical composition. For 3/2 mullite, the tetrahedrally coordinated positions will be occupied by 12.5 per cent of Si and Al atoms; for 2/1 mullite, by 20 per cent of Si and Al atoms. The chemical formula for mullite can, therefore, be written as follows:

$$Al(Si_{2-x}Al_xO_{11/2 - x/2})$$

where x varies from 1.25 to 1.40 for mullite within the interval 3/2 to 2/1.

Murthy and Hummel (34) studied the solid solution of TiO_2, Fe_2O_3, and Cr_2O_3 in synthetic mullite ($3Al_2O_3 \cdot 2SiO_2$) by measuring the changes in the lattice parameters, and unit cell volume. The maximum amount of solid solution found was 2 to 4 per cent TiO_2 at 1600°C, 10 to 12 per cent Fe_2O_3 at 1300°C, and 8 to 10 per cent Cr_2O_3 at 1600°C. They found that lattice parameters and unit cell volumes for each solid solution increased with increasing amounts of foreign ions.

Table 1 gives the lattice parameters of mullites measured by Aramski and Roy (35) and Murthy and Hummel (34). Table 2 describes the mullites listed in Table 1.

Table 1. Unit-Cell Dimensions of Mullite

No.*	a(Å)	b(Å)	c(Å)
1.	7.583	7.681	2.8854
2.	7.560	7.688	2.8840

*See Table 2.

Table 2. List of Mullites in Table 1

No.	Mullite Description
1.	Arc-fusion mullite composition $2Al_2O_3 \cdot SiO_2$
2.	Prepared from aluminum hydroxide and silicic acid. Composition $3Al_2O_3 \cdot 2SiO_2$

CHAPTER III

INSTRUMENTATION AND EQUIPMENT

Furnace

All specimen heating was done in a gas fired Ipsen automatic kiln. An Iridium vs. Iridium 60 per cent Rhodium thermocouple was used. The temperature was controlled by a Brown Electronik single-record strip chart contact controller. The strip chart contact controller continuously measures and records the temperature and initiates contact control whenever the temperature deviates from the set point by more than 10°F. An optical pyrometer was used to check the thermocouple. The optical pyrometer and thermocouple agreed within ± 10°F. Since no color difference could be detected between the thermocouple junction and the specimen, the specimen temperature differed from the thermocouple junction by less than 10°F.

X-Ray Diffractometer Unit

X-ray diffraction analysis was performed with a Norelco water cooled diffractometer unit using copper K_α radiation and a nickel filter with a wide range goniometer and sealed proportional counter. A 0.003 inch receiving slit, 1° divergence slit, and 1° scatter slit were used. A tube voltage of 40 KV and current of 24 ma were used for all work.

The pulse height analyzer (PHA) was adjusted each day with a silicon wafer for 95 per cent transmission. The detector voltage was also checked daily by the following method: an x-ray input of constant

intensity was fed into the detector; the detector voltage was slowly increased, and the output of the pulse height analyzer was observed on the strip chart. The detector voltage used was that value which gives maximum output to the recorder.

The complete list of operating conditions for qualitative and quantitative x-ray analysis are given in Table 16, Appendix A, and Table 19, Appendix B, respectively.

Optical Microscope

A Reichert Universal Camera Microscope, MeF, equipped with a low voltage Tungsten filament and Xenon Arc double lamp unit for reflected light illumination was used for the microstructural analysis.

CHAPTER IV

PROCEDURE

Two commercially available alumino-silicate refractories*, a mullite firebrick, and a high alumina refractory, that exhibit increased strength at elevated temperatures were examined with x-ray diffraction and ceramographic techniques. Standard curves for quantitative x-ray analysis of the crystalline components were prepared. The per cent of each phase present in the reference and heat treated specimens was determined from x-ray analysis and the standard curves. Mullite and alumina lattice parameter changes were also determined.

Specimen Characterization

Description

A summary of the properties of the high alumina and mullite firebrick is given in Table 3. Photomicrographs of both refractories are shown in Figures 3 and 4. The modulus of rupture data provided by Babcock and Wilcox is plotted in Figure 5. Table 4 tabulates the modulus of rupture data at the test temperatures used throughout this investigation. The modulus of rupture values given are an average of five runs. Test specimens measuring six inches by one inch by one half inch were used. The specimens were fired in a silicon carbide furnace

---

*Kaomul (mullite firebrick) and Cerox 1000 (high alumina) supplied by Babcock and Wilcox Co. in Augusta, Georgia.

Table 3. Refractory Analyses

Property		High Alumina Refractory	Mullite Firebrick Refractory
Approximate Chemical* Analysis, %			
Alumina	Al_2O_3	92.6	61.3
Silica	SiO_2	5.5	35.4
Iron Oxide	Fe_2O_3	0.5	0.9
Titania	TiO_2	1.2	2.0
Calcia	CaO	Trace	Trace
Magnesia	MgO	Trace	Trace
Alkalies, as	Na_2O	0.2	0.2
Apparent Porosity, %*		18	16
Melting Point, °F*		3560	3280
Firing Temperature, °F*		2600	> 2900
Phase Analysis, %**			
α-Alumina		79.08	16.25
Mullite***		17.21	52.75
Cristobalite		none detected	none detected
Glass		3.71	31.00

*Obtained from the Babcock and Wilcox Co.

**X-ray diffraction analysis from this investigation of room temperature specimens.

***This mullite is an arc-fusion mullite and can be represented by the formular $2Al_2O_3 \cdot SiO_2$.

containing a preheat section and a test section. The specimens were pushed through the preheat section and into the testing position at a controlled rate. A silicon carbide loading arm was attached to a lever arm.

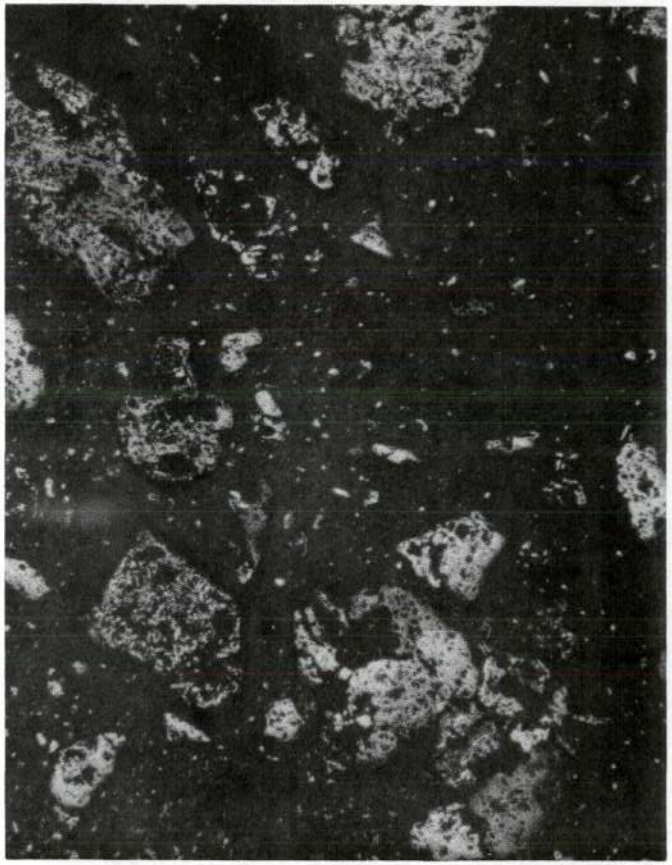

(a) 55X. Etched with H_3PO_4

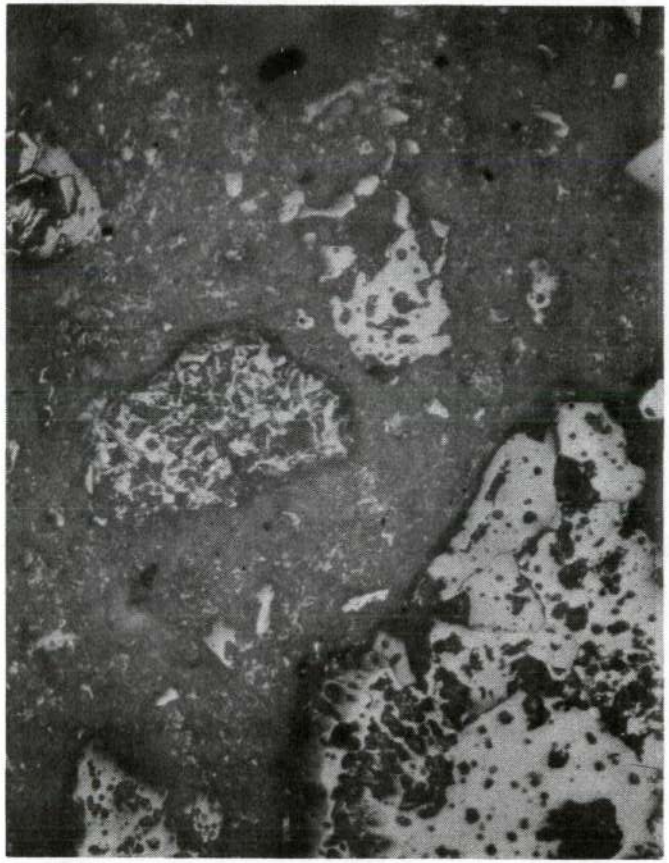

(b) 190X. Etched with H_3PO_4

Figure 3. Photomicrographs of High Alumina Refractory Before Heat Treatment.

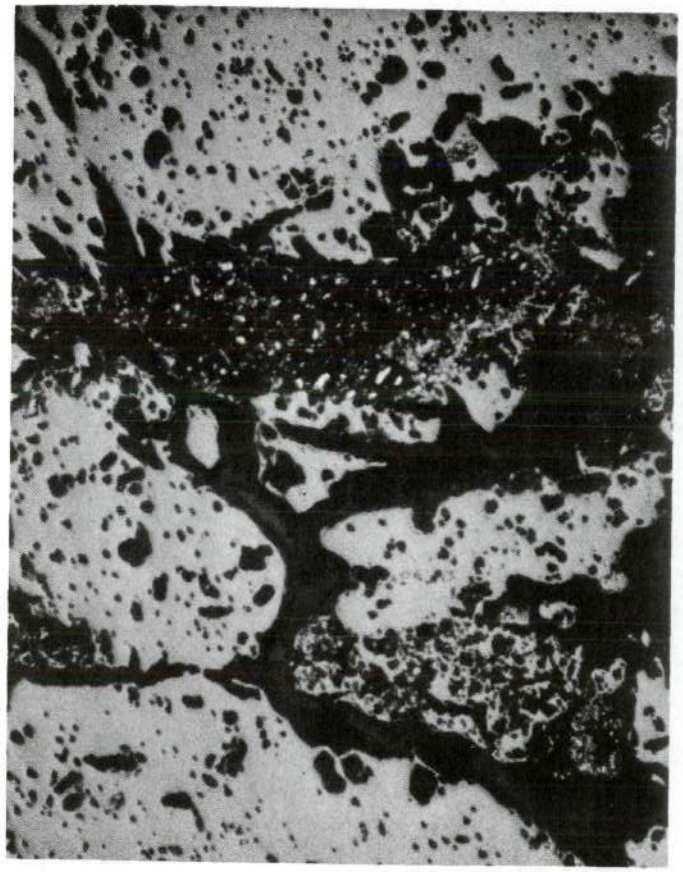

(a) 55X. Etched with H_3PO_4

(b) 190X. Etched with H_3PO_4

Figure 4. Photomicrographs of Mullite Firebrick Before Heat Treatment.

Table 4. Modulus of Rupture

Temperature °F	Modulus of Rupture, psi	
	High Alumina Refractory	Mullite Firebrick Refractory
Room Temperature	2900	2500
1800	3600*	3200*
2000	3700	3850
2300	2100	2700*
2600	1200	1100*
2800	1100	750

*These values were not furnished by Babcock and Wilcox Co., but were obtained from Figure 5.

The formula used for computing the modulus of rupture (MOR) is given below:

$$MOR = 3/2 \frac{WL}{bd^2}$$

Where: W = Load (weight of water in pounds by mechanical advantage).

L = Span of specimen in inches.

b = Breadth of specimen in inches.

d = Thickness of specimen in inches.

Specimen Selection and Treatment

Rectangular shaped specimens, approximately one half inch by one half inch by one inch, were cut from refractory brick with a diamond

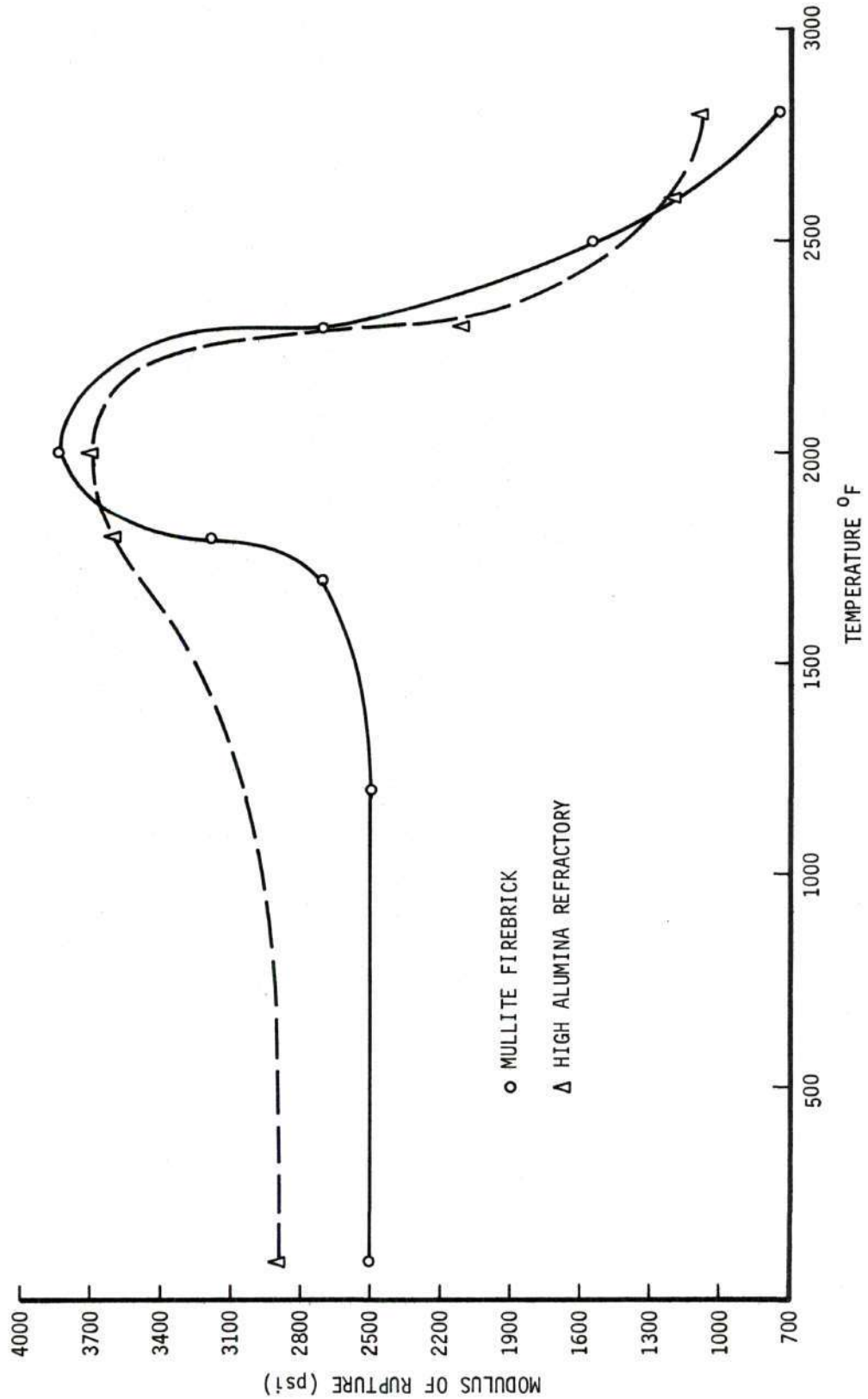

Figure 5. Effect of Temperature on Transverse Strength of Alumino-Silicate Refractories.

saw. All specimens were grouped in pairs. The specimens comprising each pair had had their larger surface in contact with one another before being cut. By using this method, the differences in composition between specimens were minimized. One specimen of each pair was chosen to be heated to a designated temperature and the other specimen to remain at room temperature for comparison. Compositional variations throughout the brick made it necessary to have more than one pair for each test temperature to ensure representative results.

The specimen pairs were arranged in five groups, and each group was heated to a different temperature. Table 5 gives the specimen identification number and corresponding test temperature for both the high alumina and mullite firebrick refractories.

Heat Treatment

The designated specimens were heated in an Ipsen gas kiln at a rate of 475°F per hour and soaked at the test temperature for three hours, quickly removed from the kiln, and quenched in water. Additional specimens were heated to 2000°F and 2300°F and allowed to cool slowly, instead of quenching, to determine if any compositional changes were reversible during the cooling cycle. These specimens contain a "C" in their notation. All the samples were placed on platinum foil to reduce any reactions with the kiln refractories.

Specimen Analysis

All specimens for x-ray analysis were ground in a mortar and pestle until they passed through a U. S. Standard 100-mesh sieve. The powder samples were then transferred to a Fisher automatic mortar grinder and ground for three additional hours. After grinding, all

Table 5. Specimen Heating Temperature

High Alumina Refractory		Firebrick Refractory	
Specimen No.	Test Temp. °F	Specimen No.	Test Temp. °F
3-Q-1	1800	1-Q-1	1800
3-Q-2	1800	1-Q-2	1800
3-Q-3	1800	1-Q-3	1800
3-Q-4	1800	1-Q-4	1800
3-Q-5	1800	1-Q-5	1800
3-Q-6	2000	1-Q-6	2000
3-Q-7	2000	1-Q-7	2000
3-Q-8	2000	1-Q-8	2000
3-Q-9	2000	1-Q-9	2000
3-Q-10	2000	1-Q-10	2000
3-Q-11	2000	1-Q-11	2000
3-Q-12	2000	1-Q-12	2000
3-Q-13	2000	1-Q-13	2000
3-Q-14	2000	1-Q-14	2000
3-Q-15	2000	1-Q-15	2000
3-Q-16	2300	1-Q-16	2300
3-Q-17	2300	1-Q-17	2300
3-Q-18	2300	1-Q-18	2300
3-Q-19	2300	1-Q-19	2300
3-Q-20	2300	1-Q-20	2300
3-Q-21	2600	1-Q-21	2600
3-Q-22	2600	1-Q-22	2600
3-Q-23	2600	1-Q-23	2600
3-Q-24	2600	1-Q-24	2600
3-Q-25	2600	1-Q-25	2600
3-Q-26	2800	1-Q-26	2800
3-Q-27	2800	1-Q-27	2800
3-Q-28	2800	1-Q-28	2800
3-Q-29	2800	1-Q-29	2800
3-Q-30	2800	1-Q-30	2800
3-C-6	2000	1-C-6	2000
3-C-7	2000	1-C-7	2000
3-C-16	2300	1-C-16	2300
3-C-17	2300	1-C-17	2300

material passed through a U. S. Standard 325-mesh sieve. The ground specimens were placed in a dryer to remove any moisture.

All specimens were analyzed with an x-ray diffractometer to determine the identity and quantity of the crystalline phases present. Aluminum sample holders were used, giving a sample surface of one centimeter by two centimeters. Preferred orientation of the alumina and mullite was minimized by using the "back loading" method (36).

The x-ray diffractometer performance was checked periodically to ensure reproducibility. A scan speed of one degree 2θ per minute and a chart speed on one-half inch per minute were used. Diffraction patterns of all specimens were run from 15 degrees 2θ to 80 degrees 2θ. The patterns were carefully checked for reflections of any phase that might be present in small amounts.

Analytical Procedures

The weight per cent of the phases present in all samples was determined by quantitative x-ray diffraction employing the internal standard method. Analysis by the internal standard method requires the addition of a constant amount of a standard substance to a mixture of the unknown composition and the preparation of standard calibration curves of known composition. The ratio of the integrated intensity (peak area) of a diffraction peak of the phases in the unknown mixture to the integrated intensity of a standard peak is obtained. Using this ratio and the standard calibration curves, the weight per cent of the phases in the unknown specimen can be determined.

Preparation of Standards

Standard mixtures of known weight per cents of alumina, mullite, and cristobalite with calcium fluoride as the internal standard were prepared. Two series of standards were made, one for the alumina and mullite combination and the other for cristobalite. Figures 6, 7, and 8 present this information, and Appendix B gives the data used in preparing the standard curves.

Calcium fluoride was chosen as the internal standard because it was obtainable in high purity, was of suitable crystalline size to give sharp diffraction peaks, and provided strong diffraction peaks near, but not overlapping, peaks of the phases to be determined.

The x-ray intensity of mullite can vary with mullite composition, impurity content, and structural disorders. Because of this intensity variation, the mullite and alumina that were used as raw materials for the two refractories were used to construct the standard curves. If this condition is not fulfilled, the resulting determinations will be satisfactory on a relative but not on an absolute scale.

Cristobalite is not a normal constituent of these refractories and was prepared from silicic acid by heating in a zirconia crucible for six hours at 1400°C and cooling slowly. This treatment gives a well-developed cristobalite whose interplanar spacings are the minimum attainable. For valid quantitative results the cristobalite in the specimens should have the same degree of order as the standard. For cristobalite with lesser degrees of order, the diffraction intensity will be reduced. Since the interplanar spacing of cristobalite formed in the specimens was very close to the interplanar spacing of the cristobalite in the

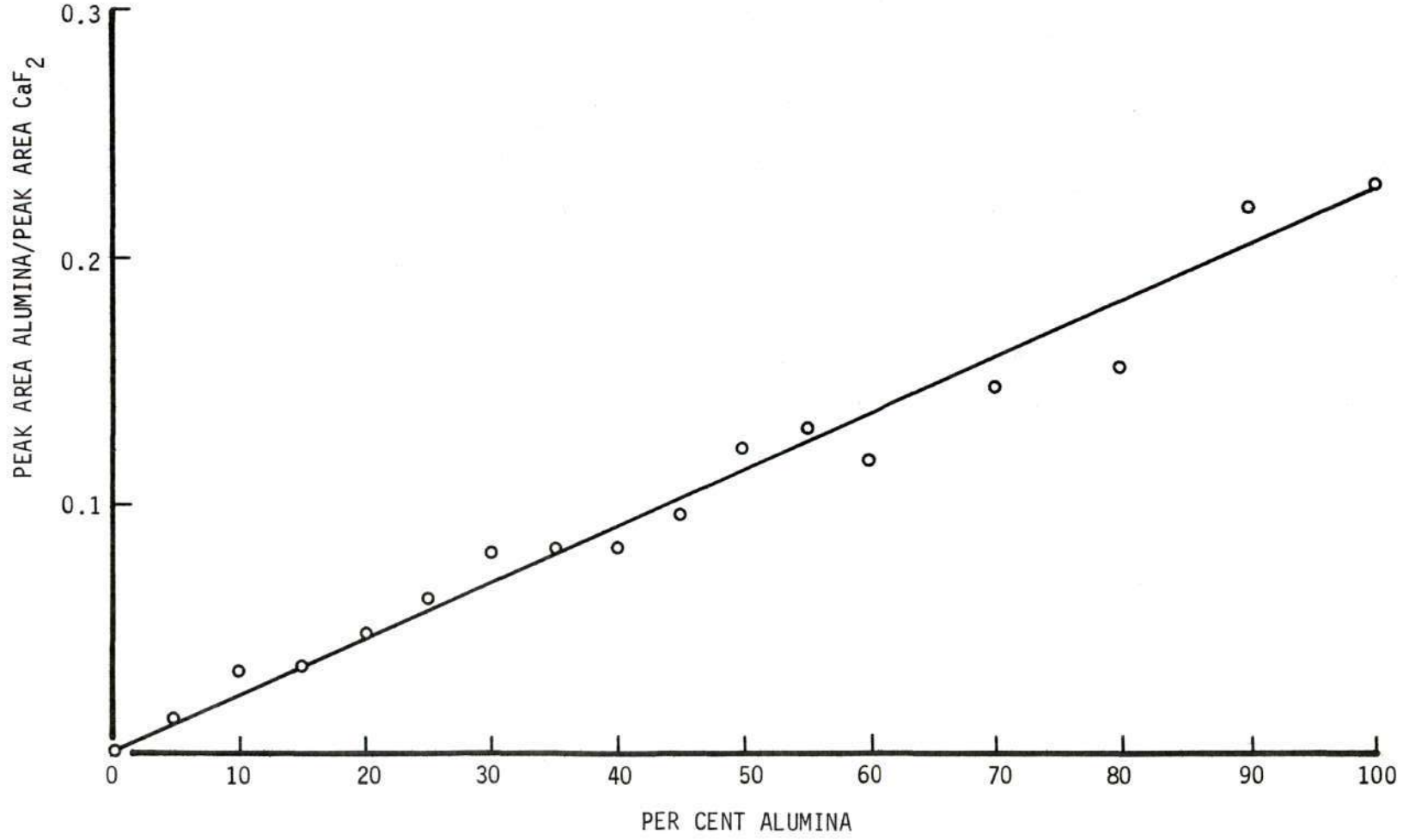

Figure 6. Alumina Standard Curve.

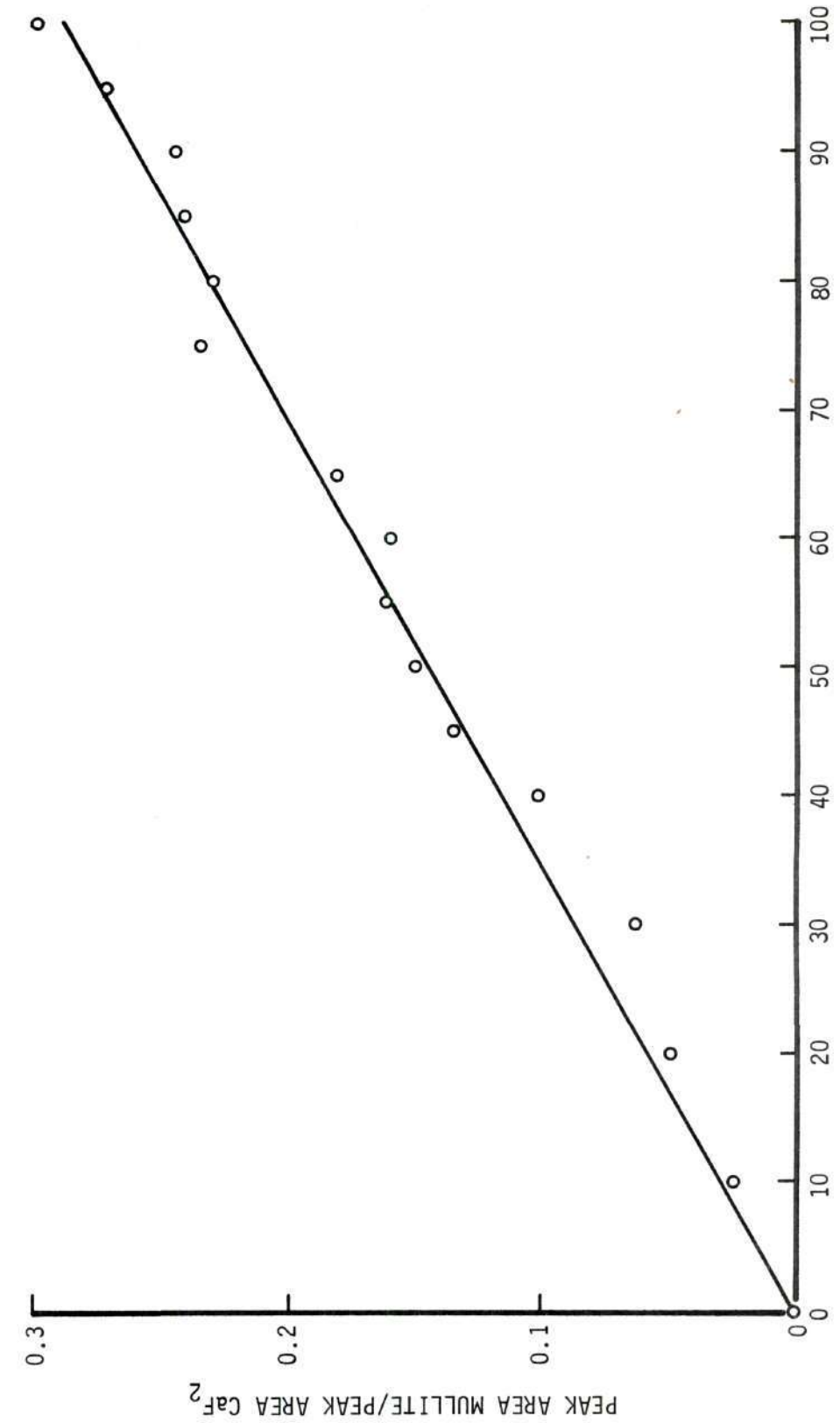

Figure 7. Mullite Standard Curve.

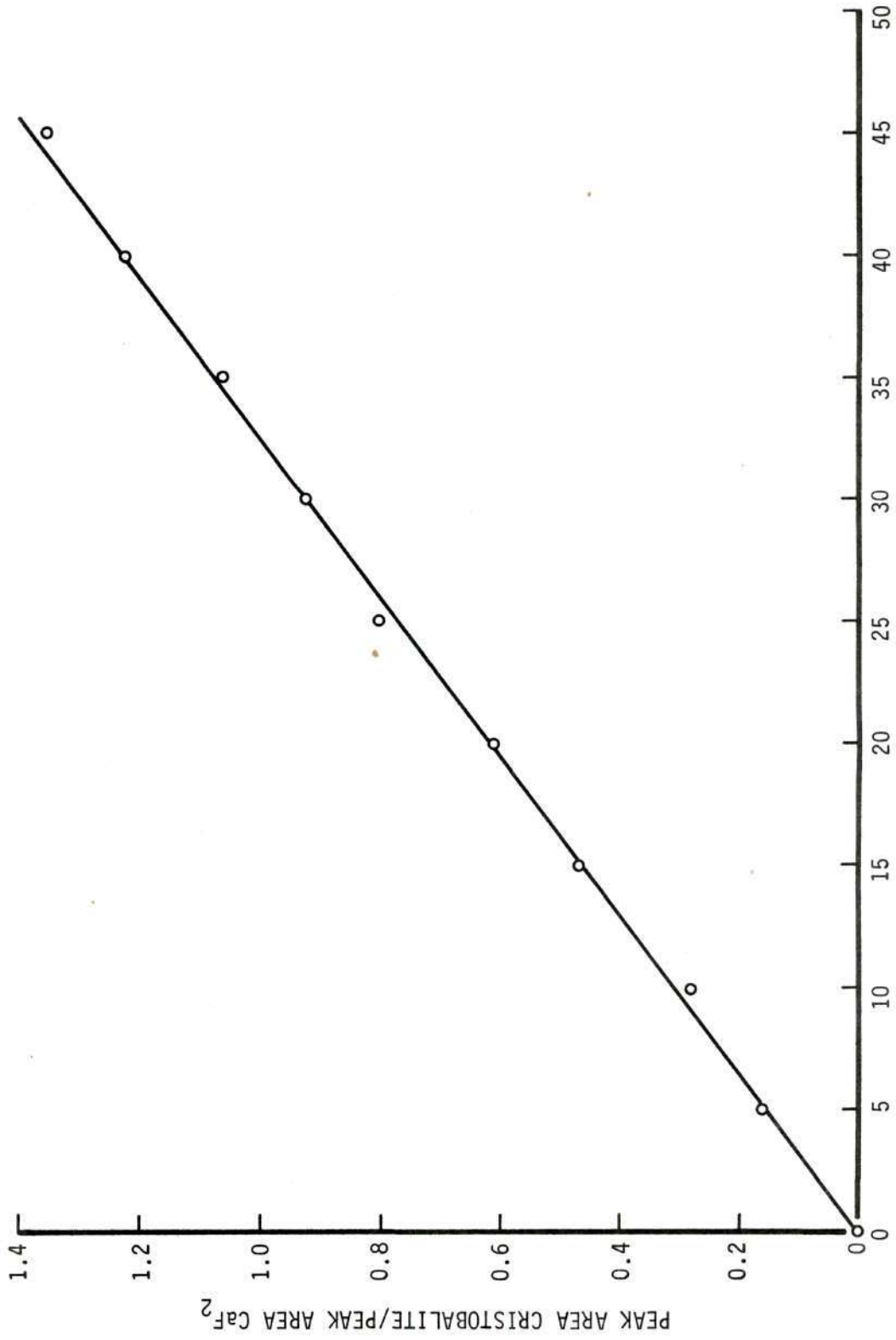

Figure 8. Cristobalite Standard Curve.

standards, no correction for intensity variation was made.

The standard curves were prepared by adding four grams of alumina and mullite or cristobalite and alumina in the correct proportions to two grams of calcium fluoride. All materials were weighed to the nearest thousandth of a gram. The standards were mixed with a Spex Mixer for onr hour to assure sample homogeneity.

The two most important factors for true and reproducible results in quantitative x-ray diffraction are small particle size and homogeneity of the sample. It is believed that the three hour grinding time was sufficient to reduce the particles to a fine enough size for consistent intensity measurements without destroying the crystalline order of the particles.

Internal Standard Method

In this method of quantitative analysis, a diffraction peak from the phase being determined is compared with a peak from a standard substance mixed with the sample in known proportions. If the amount of phase A is to be determined in a mixture of phases A, B, and C, a known amount of the original sample and standard substance, S, are mixed to form a new composite sample. From a diffraction pattern of the composite sample, the integrated intensity, I_A, of a particular peak from phase A is given by:

$$I_A = \frac{K_1 C_A'}{\mu_m}$$

Where: K_1 = a constant.

C_A' = volume fraction of phase A in the composite sample.

μ_m = linear absorption coefficient of the mixture.

and the intensity of a particular peak from the standard, S, by

$$I_S = \frac{K_2 C_S}{\mu_m}$$

Where: C_S = volume fraction of S in the composite. Division of one expression by the other gives

$$\frac{I_A}{I_S} = \frac{K_1 C'_A}{K_2 C_S} \tag{1}$$

Since the volume fraction of each phase is a function of the weight per cent and densities of all the phases present in the composite, the following expression can be obtained:

$$\frac{C'_A}{C_S} = \frac{W'_A \rho_S}{W_S \rho_A}$$

Where: W'_A = weight fraction of phase A in the composite.

W_S = weight fraction of the standard in the composite.

ρ = density of the designated phases.

Substitution of this relation into equation (1) gives

$$\frac{I_A}{I_S} = K_3 W'_A \tag{2}$$

if W_S is kept constant in all the composite samples. The relationship between the weight fraction of A in the original, W_A, and the composite sample is:

$$W'_A = W_A (1 - W_S) \tag{3}$$

Combination of equation (2) and (3) gives

$$\frac{I_A}{I_S} = K_4 W_A \qquad (4)$$

The intensity ratio of a diffraction peak from phase A and standard S is, therefore, a linear function of W_A, the weight fraction of A in the original sample. Figures 6, 7, and 8 indicate this behavior.

The constants, K, in the expressions are used to represent the factors controlling the integrated intensities of reflections, which are constant and independent of concentration (37).

Theoretically, calibration curves for the internal standard method are straight lines. Therefore, in order to obtain the best possible fit, the linear regression procedure, Appendix C, was used to calculate a least squares fit to the data as shown in Figures 6, 7, and 8.

Preparation of Standard Curves

Quantitative x-ray work was done using the experimental conditions outlined in Appendix B. The reflections used in the quantitative analysis of standards are listed in Table 6. These reflections satisfied the requirements given previously for the internal standard method. The reflections of the materials to be analyzed were chosen as close as possible to the reflection of the internal standard to avoid intensity variations caused by the atomic scattering factor.

In preparing the standard calibration curves, a series of three to five determinations of the ratios, A_a/A_f, A_m/A_f, and A_c/A_f, where A is the integrated reflection area and the subscripts a, m, c, and f denote alumina, mullite, cristobalite and fluorite, for each mixture was obtained.

Table 6. X-Ray Reflections Used in Quantitative Phase Determinations

Material	Reflection Indices	2θ Value	Lattice Spacing (Å)
Alumina	(110)	37.75	2.3809
Mullite	(110)	16.35	5.5659
Cristobalite	(111)	21.75	4.0826
Calcium Fluoride	(111)	28.30	3.1534

The average ratios were plotted against the weight per cent of alumina, mullite, and cristobalite respectively. In order for the results to be more representative of the standard mixtures, the powder was poured from the specimen holder, and the sample remounted between each measurement.

Quantitative Phase Determination

Experimental conditions were the same as used for determining the standard calibration curves except a scale factor of 5×10^2 was used. The x-ray reflections used are given in Table 6. Each specimen was run at least twice, the specimen being remounted in the holder before each run. The integrated intensities were measured with a compensating planenometer and the ratio of the peak areas calculated. The weight per cent of each crystalline phase was determined, and the weight per cent of the noncrystalline phase were obtained by difference.

Intensity variations between runs of the same specimen were due to preferred orientation. Intensity variations between different room

temperature specimens were due to preferred orientation and lack of homogeneity of the brick.

The possibility of increasing the alumina content of the specimen from the weak of the alumina mortar and pestle was checked by grinding silicon carbide for three hours. The silicon carbide was checked by x-ray diffraction for alumina before and after grinding. No alumina was detected.

Mullite Parameter Changes

Lattice parameter changes in mullite caused by compositional changes and strain were studied with x-ray diffraction. X-ray diffraction patterns of selected specimens of both high alumina and mullite firebrick refractories were run. The experimental conditions were the same as those given in Appendix A with the exception of a scan speed of 1/4° 2θ/ minute and a time constant of 4. All patterns were run from 15° 2θ to 80° 2θ. Lattice parameters were calculated by the method shown in Appendix F.

The intensity ratio of the (210) and (120) reflections of mullite was used to study changes in the mullite composition at various temperatures. This ratio gives an indication of the composition of mullite since a low value indicates the presence of free alumina in the structure, i.e., a mullite corresponding to the formula $2Al_2O_3 \cdot SiO_2$ (25). The effect of compositional changes on the lattice parameters of mullite made it impossible to obtain an accurate measurement of the strain.

Alumina Parameter Changes

The alumina lattice parameters were calculated for the alumina used as a raw material and the alumina in both refractories at each

test temperature. A sample calculation is shown in Appendix F.

Strain measurements of alumina were made by x-ray diffraction on the (124) plane. The strain values reported are those normal to this plane. The experimental conditions were the same as for the lattice parameter determinations.

Assuming the alumina used as a raw material is unstrained, the crystal strain is obtained from the equation (38):

$$\varepsilon = -\Delta\theta \cot \theta \qquad (5)$$

Where: ε = strain in crystal.

θ = Bragg angle.

$\Delta\theta$ = displacement of Bragg angle.

Ceramographic Technique

Selected specimens chosen for microstructure studies were mounted and polished. Silicon carbide bonded paper in grit sizes of 180, 320, and 600 was used for the fine grinding stage. Five micron alpha-alumina and one micron diamond paste were used in the rough polishing. The final polishing was done with 0.3 micron alpha-alumina. Relief polishing of the specimens was accomplished with 0.3 micron alpha-alumina on a micro-cloth. After polishing, the specimens were etched for five minutes in hot phosphoric acid.

CHAPTER V

RESULTS AND DISCUSSION

The primary objective of this research was to study compositional changes of alumino-silicate refractories at elevated temperatures, and use these results to modify or substantiate previously proposed theories for increased strength at elevated temperatures. The effect of the composition changes on strength are discussed. In addition to studying changes in the amount of the various phases in the refractories, changes in the mullite composition and strain in the alumina were measured and microstructure studies were performed. The combined results from these studies and previous work are used to determine the reasons for strength changes with temperature of the refractories investigated.

Compositional Analysis

The results of the compositional analysis performed on room temperature and heated specimens using the internal standard x-ray diffraction procedure are given in Tables 21 and 22 of Appendix E. The average composition obtained from all the analyses of the mullite firebrick and high alumina refractory are given in Tables 7 and 8, respectively. All specimens contained α-alumina and mullite. No cristobalite was detected in any of the high alumina specimens, however, quartz was detected in two of the high alumina room temperature specimens and one specimen fired to 2000°F. Cristobalite was formed in the mullite firebrick heated to 2000°, 2300°, and 2600°F. Cristobalite was also detected in one room temperature mullite firebrick specimen. Small amounts of quartz were

Table 7. Average Composition of Mullite Firebrick Refractory

Temperature °F	Per Cent Mullite	Per Cent Alumina	Per Cent β-Cristobalite	Per Cent Glass
Room Temperature	52.75	16.25	none detected	31.00
1800	54.07	13.75	none detected	32.18
2000	51.04	14.45	7.25	27.26
2300	49.83	13.62	11.93	24.62
2600	51.27	14.97	9.08	24.68
2800	49.74	15.46	none detected	34.80

Table 8. Average Composition of High Alumina Refractory

Temperature °F	Per Cent Mullite	Per Cent Alumina	Per Cent Glass
Room Temperature	17.21	79.08	3.71
1800	17.44	78.47	4.09
2000	16.43	76.07	7.50
2300	18.66	77.70	3.64
2600	16.60	77.88	5.52
2800	16.45	79.05	4.50

found in two mullite firebrick room temperature specimens and one mullite firebrick fired to 2800°F.

Compositional Changes Between Room and Elevated Temperatures

The lack of homogeneity of the refractories, shown by the variable compositions in Tables 21 and 22, made it impossible to compare the average composition at each test temperature with the average room temperature composition. Compositional changes were obtained by comparing the heated specimens to their corresponding room temperature specimens. This did not entirely eliminate the error of compositional variation, but it did minimize this error. The compositional changes at elevated temperatures of the mullite firebrick examined are given in Table 9 and Figure 9. The compositional changes at elevated temperatures of the high alumina refractory are given in Table 10 and Figure 10.

A statistical decision was made on the significance of the differences in the compositional mean values of the reference and test specimens. A significance level of 0.10 was chosen, i.e., a 90 per cent confidence level that the right decision was made. The statistical analysis showed that changes of less than one per cent in the mullite firebrick and 0.60 per cent in the high alumina refractory were not significant. This does not state that any change smaller than these values did not occur, but rather that they were unable to be detected with 90 per cent confidence (39).

The mullite and glass content of the mullite firebrick increased from room temperature to 1800°F, while the alumina content decreased. Above 1800°F the mullite content was always less than at room temperature.

Table 9. Composition Changes of Mullite Firebrick Between Room and Test Temperature

Temperature °F	Per Cent Mullite	Per Cent Alumina	Per Cent Cristobalite	Per Cent Glass
1800	+1.25	-3.70	none detected	+2.45
2000	-0.38	-1.34	+7.25	-5.53
2300	-3.24	-1.32	+11.93	-7.37
2600	-1.91	-0.78	+9.08	-6.39
2800	-3.53	-1.85	none detected	+5.38

Table 10. Composition Changes of High Alumina Refractory Between Room and Test Temperature

Temperature °F	Per Cent Mullite	Per Cent Alumina	Per Cent Glass
1800	+0.58	+0.99	-1.52
2000	-1.09	-2.63	+3.72
2300	+2.23	-2.28	+0.05
2600	-0.91	-0.77	+1.68
2800	-1.30	-1.53	+2.83

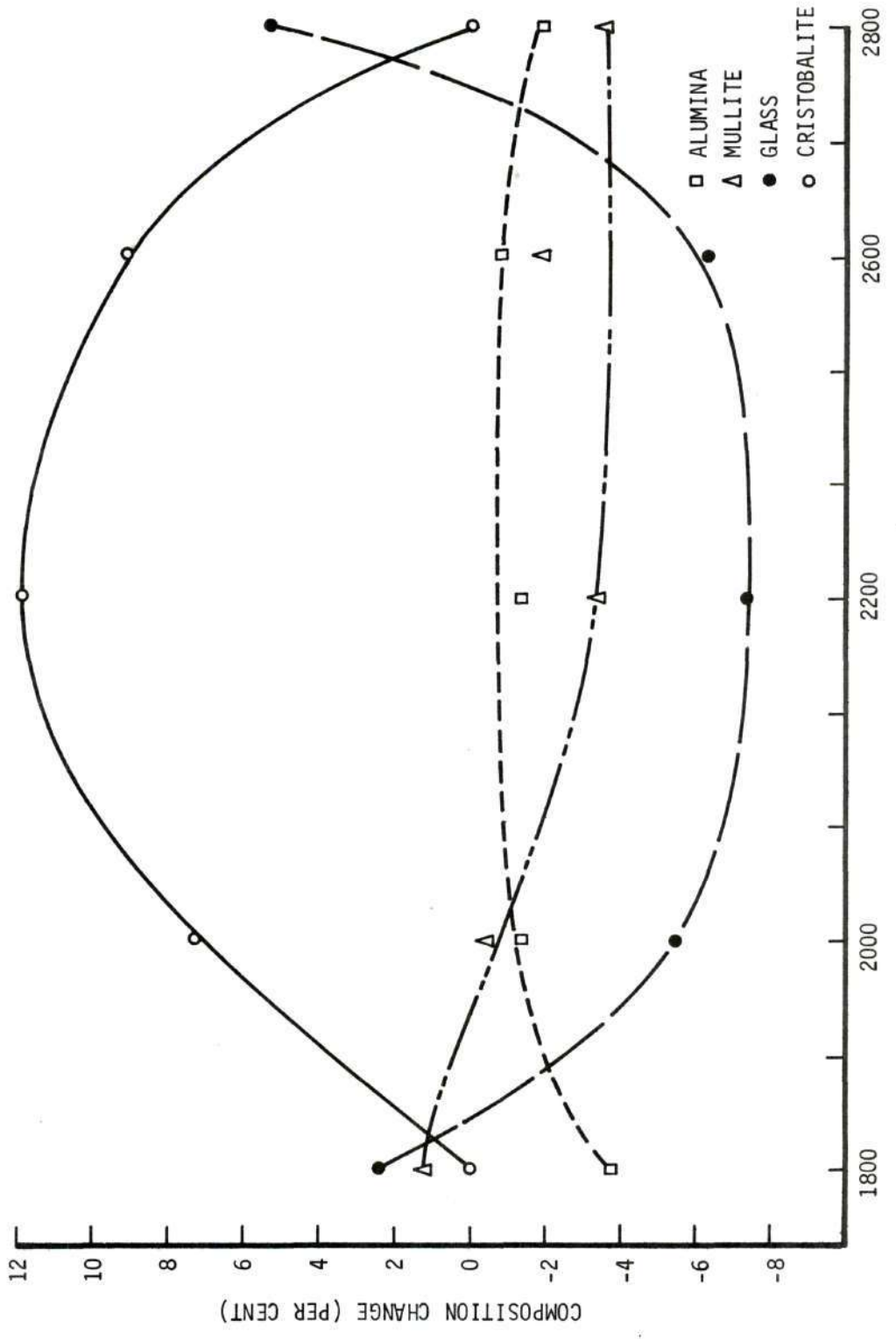

Figure 9. Composition Changes of Mullite Firebrick Between Room and Test Temperature.

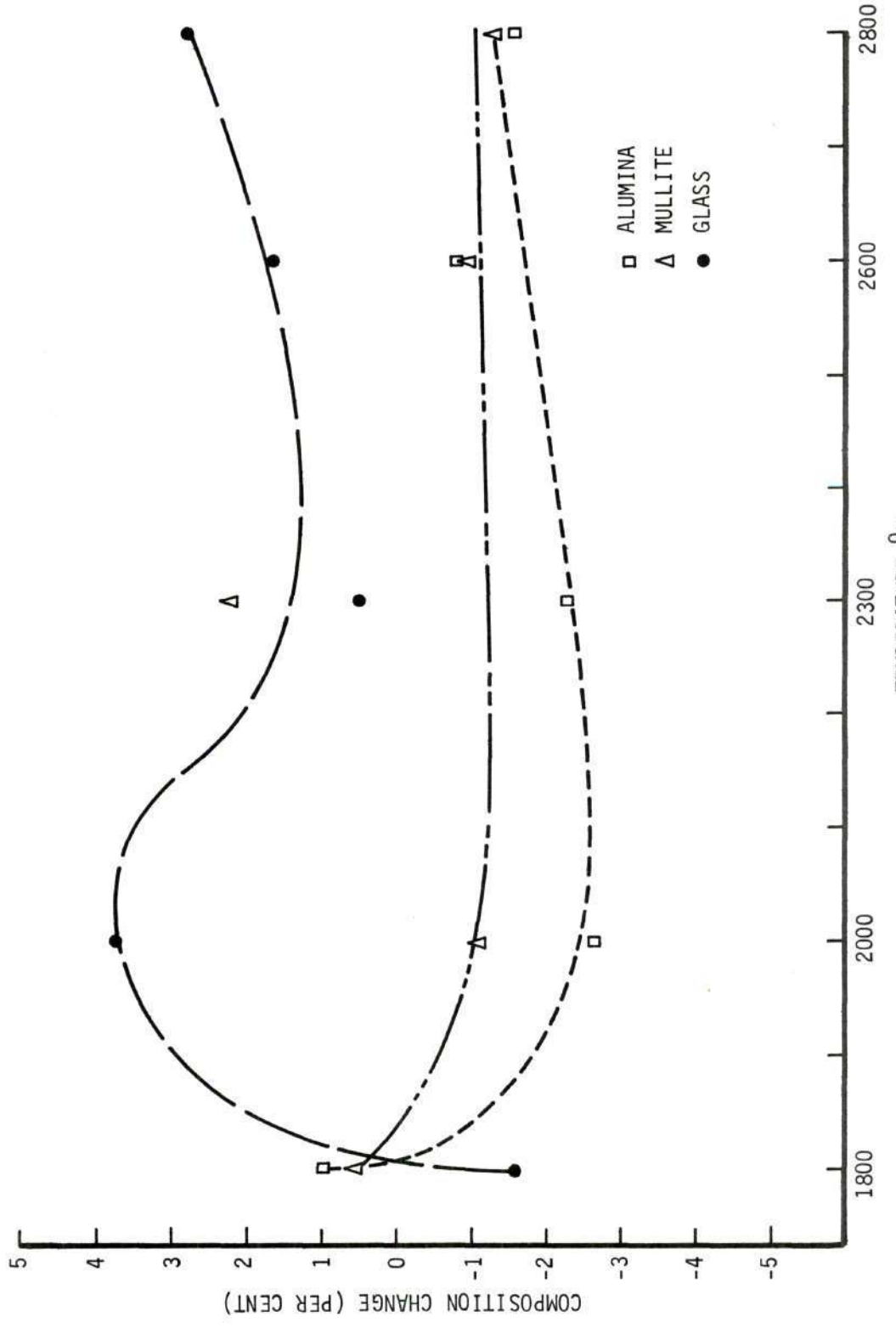

Figure 10. Composition Changes of High Alumina Refractory Between Room and Test Temperature.

The alumina content increased until 2600°F and then decreased. However, at all temperatures the amount of crystalline alumina in the mullite firebrick was less than at room temperature. Cristobalite formation was detected above 1800°F and had reached 7.25 per cent at 2000°F. The cristobalite content reached a maximum at 2300°F and decreased until none was detected at 2800°F. The glass content displayed just the reverse behavior, reaching the minimum value at 2300°F.

In the high alumina refractory the amount of mullite and alumina increased to 1800°F, and the glass content decreased. Above 1800°F the alumina content was always less than at room temperature. If the mullite change at 2300°F is disregarded, the mullite content above 1800°F was always less than at room temperature. The glass content above 1800°F was always greater than at room temperature.

Devitrification of the Glassy Phase

The largest compositional change occurring in the mullite firebrick was the formation of cristobalite from the devitrification of the metastable glassy phase. The mechanisms for the cristobalite formation are discussed below.

The rate of devitrification of the glassy phase is a function of the temperature; the surface area per unit weight of the glassy phase, since devitrification initiates from the surface; the structural stability of the glass; and the mineralizers present. In order for cristobalite to form from the glassy phase, considerable motion of the silica tetrahedra is necessary. An exceptionally high viscosity of a glassy phase indicates a high degree of association and lack of free mobility of the tetrahedra, therefore reducing the rate, and hence the

amount of cristobalite formed.

The surface area per unit weight of the glassy phase can be influenced by porosity in the glassy phase; small crystallites dispersed throughout the glassy phase; or having the glassy phase as a continuous thin film around the crystalline particles. Impurities tend to increase the amount and rate of devitrification of the glassy phase by decreasing the viscosity and increasing the mobility of the silica tetrahedra or, by producing centers of ionic asymmetry which are effective in causing nucleation. High silica glasses with added alumina have been shown to devitrify to cristobalite more rapidly than silica glass without alumina (40).

The glassy phase in the mullite firebrick is probably in continuous thin films and globules, therefore, having a smaller surface area per unit weight than in the high alumina refractory. Cristobalite was formed in the mullite firebrick heated to 2000, 2300, and 2600°F (Table 7, Figure 9). The cristobalite content of the mullite firebrick reached a maximum at 2300°F and then fell to such a small amount that none could be detected at 2800°F. The initial formation of cristobalite at 2000°F could in part be controlled by the exsolution of alumina from mullite. From the lattice parameters calculated for mullite in the mullite firebrick, it will be shown that the alumina content of mullite is reduced. It is possible that the excess Al_2O_3 at the mullite-glass interface acts as a nucleating agent for the precipitation of cristobalite from the glass.

Above 2300°F the increased glass content and accompanying decrease in cristobalite are understandable from phase equilibria considerations.

The bulk composition of the mullite firebrick lies on the silica side of the mullite region in the system Al_2O_3 - SiO_2. At 2900°F this composition will consist only of a mullite solid solution and a silica rich liquid at equilibrium. The impurity content (Table 3) and non-equilibrium nature of this refractory prevent a detailed analysis, however, these factors will lower the solidus temperature and lead to the formation of a stable glass phase in the refractory at temperatures well below 2900°F. At temperatures above 2300°F the quantity and silica content of the equilibrium liquid increase and, therefore, reduce the SiO_2 available for devitrification.

The effect of the cooling cycle on compositional changes was studied on mullite firebrick specimens heated to 2000° and 2300°F and cooled slowly. The cristobalite content of mullite firebrick fired to 2000° and 2300°F for three hours and cooled slowly was 7.7 per cent and 13.5 per cent, respectively. These are essentially the same values as obtained for the quenched specimens.

In the high alumina refractory, which contains much less glass than the mullite firebrick, it is most likely that the glass forms a continuous film around the alumina and mullite grains and, therefore, has a maximum surface area. Since no cristobalite was detected in the heated specimens of the high alumina refractory, this would indicate a highly stable glass possessing a high viscosity and a low impurity concentration. The relative changes in alumina content of the glassy phase can be seen from quantitative x-ray diffraction data shown in Table 10. The increasing alumina content of this glass provides evidence of its high stability.

Lattice Parameter Changes

The lattice parameter changes of mullite and alumina in both refractories were determined. The lattice parameter changes of the mullite furnish information on the compositional changes of the mullite.

The major cause of variation in unit cell dimensions of mullite is a change in the Al_2O_3/SiO_2 ratio (35). In general, Al substitution for Si in the mullite lattice increases the a and c dimensions of the unit cell. The effect on the b dimension is less systematic. The two methods used to determine the Al_2O_3/SiO_2 ratio change were lattice parameter measurements by x-ray diffraction and measurements of the (210)/(120) reflection ratio of mullite.

A change in the Al_2O_3/SiO_2 ratio is not the only cause of mullite parameter variations. Parameter changes are also observed in heat treated mullites that have been quenched. The changes probably reflect Al-Si disorder at high temperatures (35). As the temperature increases, the a and c lattice parameters increase. An additional cause of changes in mullite lattice parameters is solid solution of such materials as TiO_2, Fe_2O_3, and Cr_2O_3 (34). The lattice parameters of mullite increase with increasing amounts of the foreign oxides.

Mullite Parameter Changes in Mullite Firebrick

The mullite lattice parameters at each test temperature are given in Table 11. The a and c lattice parameters of the mullite used as the raw material were 7.576 Å and 2.888 Å, respectively. These values correspond to reported values of mullite of the composition $2Al_2O_3 \cdot SiO_2$ (35). This is not too surprising since the original mullite was an

arc-fused product, which is almost always of the composition $2Al_2O_3 \cdot SiO_2$.

A major decrease in the a parameter and increase in the (210)/(120) ratio between the initial fused mullite (raw material) and the mullite in the room temperature bricks were noticed. These changes indicate a loss of Al_2O_3 from the mullite. Subsequent parameter and (210)/(120) ratio changes were small compared to the changes between the raw mullite and the mullite in the room temperature brick. The a parameter values and (210)/(120) ratio give some evidence of further loss of Al_2O_3 from the mullite at the test temperatures.

The Al_2O_3 exsolved from the mullite during the initial firing is available at the mullite-glass interface and undoubtedly aids in the precipitation of cristobalite.

Mullite Parameter Changes in High Alumina Refractory

The mullite lattice parameters for the mullite in the high alumina refractory are given in Table 11. The mullite a parameter decreased and the (210)/(120) ratio increased between the raw mullite and the mullite in the room temperature specimens. Subsequent parameter and (210)/(120) ratio changes were small compared to this. The mullite a parameter and (210)/(120) ratio indicate a small decrease in Al_2O_3 content in the mullite with increasing test temperature.

Alumina Lattice Parameter Changes

The lattice parameters of alumina in both the mullite firebrick and high alumina refractories are given in Table 12. The lattice parameter values of alumina in both refractories at some test temperatures differed from the accepted ASTM values. The best explanation for this

Table 11. Mullite Lattice Parameters and (210)/(120) Peak Ratio

Sample	Temp. °F	a(Å)	b(Å)	c(Å)	V(Å^3)	$\frac{(210)}{(120)}$
			± 0.001 Å			
Original Mullite	Room Temp.	7.576	7.689	2.888	168.2	1.15
Firebrick	Room Temp.	7.539	7.696	2.888	167.5	1.38
Firebrick	1800	7.536	7.694	2.892	167.7	1.42
Firebrick	2000	7.543	7.694	2.891	167.8	1.37
Firebrick	2300	7.537	7.696	2.887	167.5	1.39
Firebrick	2600	7.541	7.694	2.890	167.7	1.38
Firebrick	2800	7.538	7.699	2.889	167.6	1.43
High Alumina	Room Temp.	7.562	7.686	2.894	168.2	1.38
High Alumina	1800	7.565	7.707	2.885	168.2	1.31
High Alumina	2000	7.549	7.694	2.889	167.8	1.35
High Alumina	2300	7.539	7.708	2.893	168.1	1.34
High Alumina	2600	7.540	7.707	2.890	167.9	1.33
High Alumina	2800	7.547	7.699	2.887	167.7	1.36

difference is strain of the alumina crystals caused by differences in thermal expansions of the components of the system.

The alumina a parameter in both refractories increased with heat treatment. The behavior of the c parameter was less systematic than the a parameter, but generally decreased with heat treatment.

Strain in Alumina

It is known that the polycomponent nature of a ceramic body may lead to the presence of strains due to differences in the thermal expansion coefficients of the phases. These strains should not be removed by annealing and should not deform the body on a macroscopic scale.

Alumina was the only crystalline phase suitable for strain measurements, since a change in lattice spacing of mullite can also be caused by compositional changes. The values of strain in the alumina given in Table 13 were obtained from the displacement of the (124) reflection of quenched specimens from the (124) reflections of the raw alumina.

Fulrath (13) believes that internal stress development in crystal-glass systems is connected to wetting of the crystal by the glass. If Fulrath's theory is correct, the fact that the alumina is in tension indicates that the glass wets the alumina, and the thermal expansion of alumina is greater than the glass. According to Fulrath's model, this condition would imply that the glass was in compression. This situation where the grains are under tensile stresses and the glassy matrix under compressive stresses is unfavorable for the propagation of Griffith's flaws, since the compressive stresses are barriers in their path. The strain data for alumina, Table 13, show the alumina to be in tension in

Table 12. Alumina Lattice Parameters

Sample	Temperature °F	Unit Cell Parameters a(Å) ±0.001 Å	c(Å)	V(Å^3)
Original Alumina	Room Temperature	4.758	13.005	254.9
Firebrick	Room Temperature	4.760	12.998	257.1
Firebrick	1800	4.762	12.991	257.1
Firebrick	2000	4.762	12.998	257.2
Firebrick	2300	4.759	13.005	257.1
Firebrick	2600	4.761	12.985	256.8
Firebrick	2800	4.761	12.985	256.8
High Alumina	Room Temperature	4.759	12.991	256.7
High Alumina	1800	4.759	12.985	256.6
High Alumina	2000	4.760	12.946	256.0
High Alumina	2300	4.761	13.005	257.2
High Alumina	2600	4.759	12.991	256.8
High Alumina	2800	4.759	12.991	256.7

Table 13. Strain of Alumina Crystals

Material	Temperature °F	Δθ (degrees)	Strain* (Å)
Firebrick	Room Temperature	0.020	-3.054×10^{-2}
Firebrick	1800	0.020	-3.054×10^{-2}
Firebrick	2000	0.030	-4.587×10^{-2}
Firebrick	2300	0.015	-2.229×10^{-2}
Firebrick	2600	0.025	-3.818×10^{-2}
Firebrick	2800	0.030	-4.587×10^{-2}
High Alumina	Room Temperature	0.005	-7.627×10^{-3}
High Alumina	1800	0.005	-7.627×10^{-3}
High Alumina	2000	0.010	-1.526×10^{-2}
High Alumina	2300	0.015	-2.289×10^{-2}
High Alumina	2600	0.005	-7.627×10^{-3}
High Alumina	2800	0.010	-1.526×10^{-2}

*Negative value indicates tension.

both refractories at all test temperatures. These results and the increasing strength of both refractories up to 2000°F support Fulrath's theory.

Microstructure Study

Studies of the microstructure of the two refractories helped verify some of the hypotheses of this investigation. Figures 3, 11, and 12 show the high alumina refractory to consist mostly of small alumina particles and a few mullite particles. Direct bonding exist between some particles, while a thin lens of glass separates others. Figure 12B shows a high alumina refractory broken at 2000°F. It should be noted that the fracture path was contained entirely in the glassy phase. This indicates that the glass-crystal interface was stronger than the glassy phase itself.

The mullite firebrick is shown in Figures 4, 13, and 14. This refractory consists of large mullite grains and alumina particles separated by large areas of glass. Figure 14A shows fissures and porosity between alumina grains and the matrix after heating to 2600°F. Cracks in a large mullite grain, heated to 2600°F, are shown in Figure 14B.

Causes of Strength Changes

The relationship between compositional and strength changes in the mullite firebrick and high alumina refractory generated during this study is evaluated in conjunction with alternative approaches and theories of increased strength. The two refractories are considered separately, as their behavior is distinctly different.

(a) 960X Etched with H_3PO_4

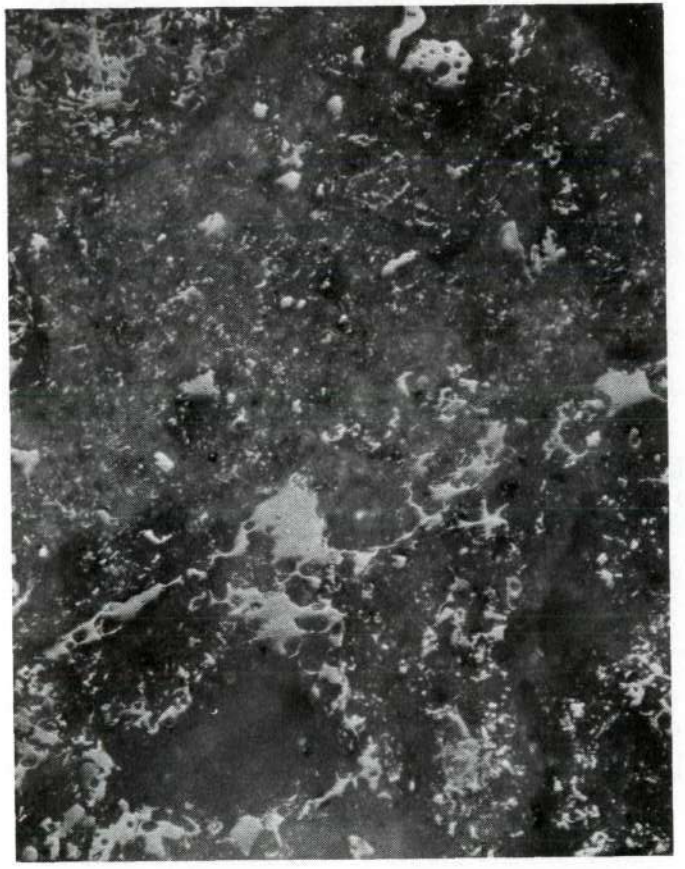

(b) 192X Etched with H_3PO_4

Figure 11. Photomicrographs of High Alumina Refractory Before Heat Treatment.

(a) 480X. 2000°F. Etched with H_3PO_4

(b) 55X. Broken at 2000°F. Etched with H_3PO_4

Figure 12. Photomicrographs of High Alumina Refractory.

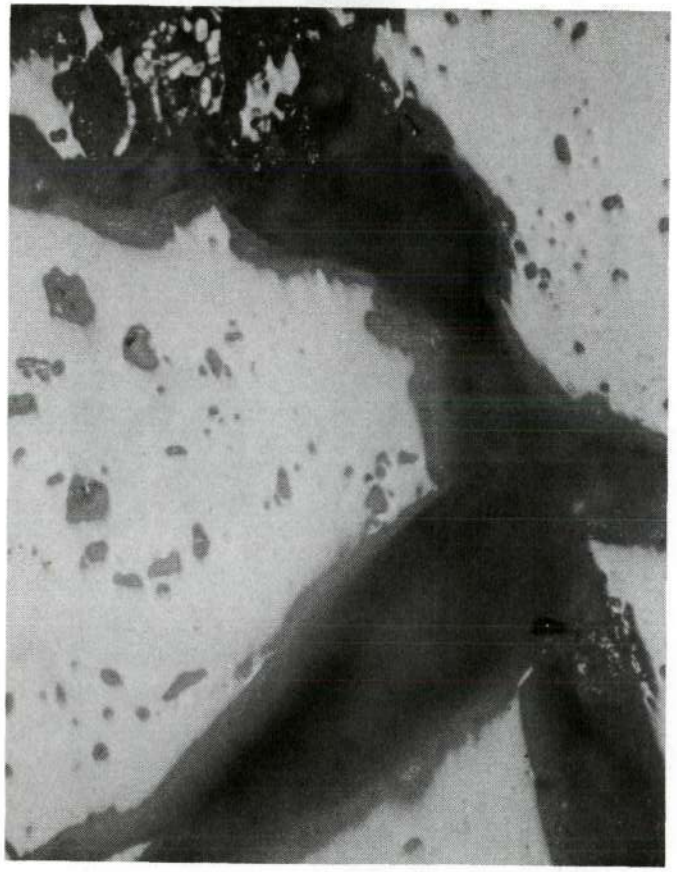

(a) 192X. Etched with H_3PO_4

(b) 192X. Etched with H_3PO_4

Figure 13. Photomicrographs of Mullite Firebrick Heated to 2600°F.

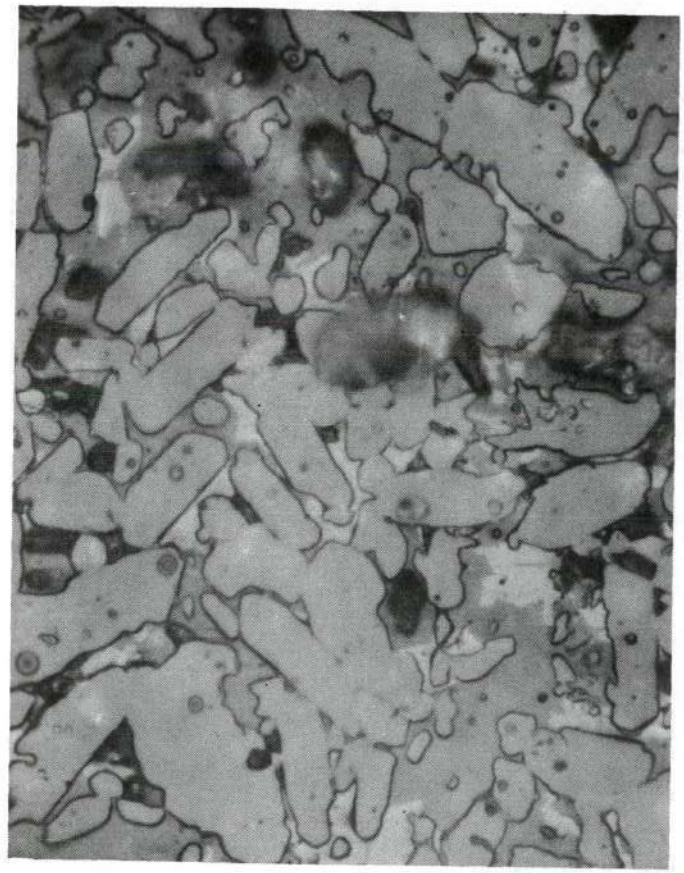

(a) 800X. Etched with H_3PO_4

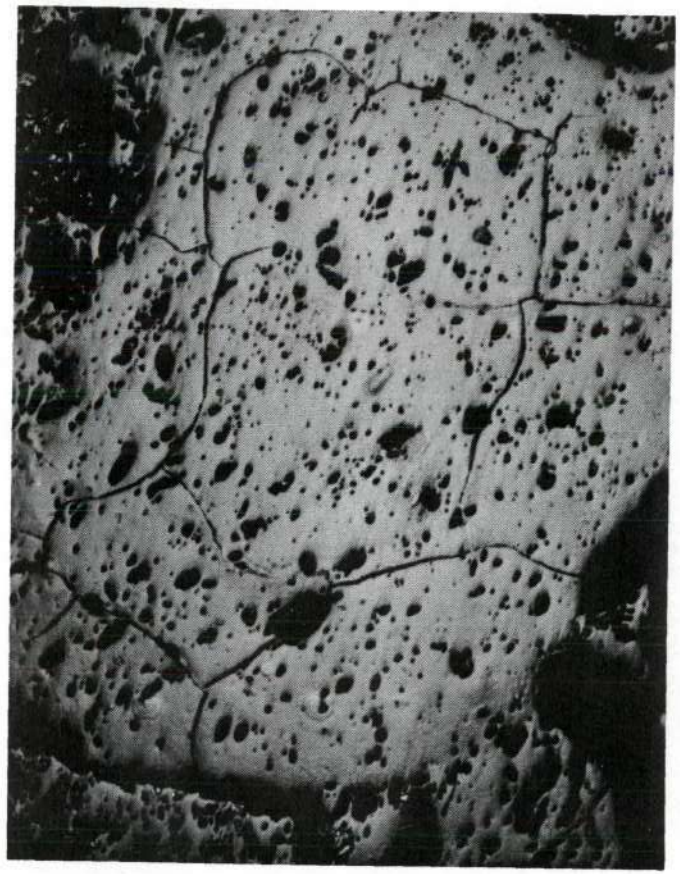

(b) 55X. Etched with H_3PO_4

Figure 14. Photomicrographs of Mullite Firebrick Heated to 2600°F.

Mullite Firebrick

The strength and major compositional changes with temperature are presented in Figure 15. As the strength increased 54 per cent, the cristobalite increased seven per cent.

The exact means by which the cristobalite affects the strength of the mullite firebrick is unknown. Since cristobalite formation occurs at approximately the same temperature that the strength begins to increase, there is undoubtedly some correlation. The ways by which the cristobalite could increase the strength are by causing an increase in the viscosity of the glassy phase at a constant temperature (23), and the formation of a cristobalite link between mullite grains originally separated by a thin film of glass (5). Also, it should be noted that as the cristobalite content increased, the glass content decreased. This increase in crystalline content of the refractory would definitely affect the strength.

The decrease in glass content at 2000°F is undoubtedly a major cause for the increased strength at this temperature. The changes in the amount of alumina and mullite were small compared to the cristobalite and glass changes. Therefore, their role as nucleating agents for the cristobalite was more influential on strength increases than the variation in quantity of these phases.

In summary, the increase in strength at 1800°F is caused by improved cohesive forces between particles; closure of cracks; and possibly small compositional changes in the glassy phase. For cohesive forces between particles to be present, the liquid must wet the solid. Strain measurements on alumina indicate the glassy phase has wet the alumina, and a bond has been established. Although no direct observation of closure

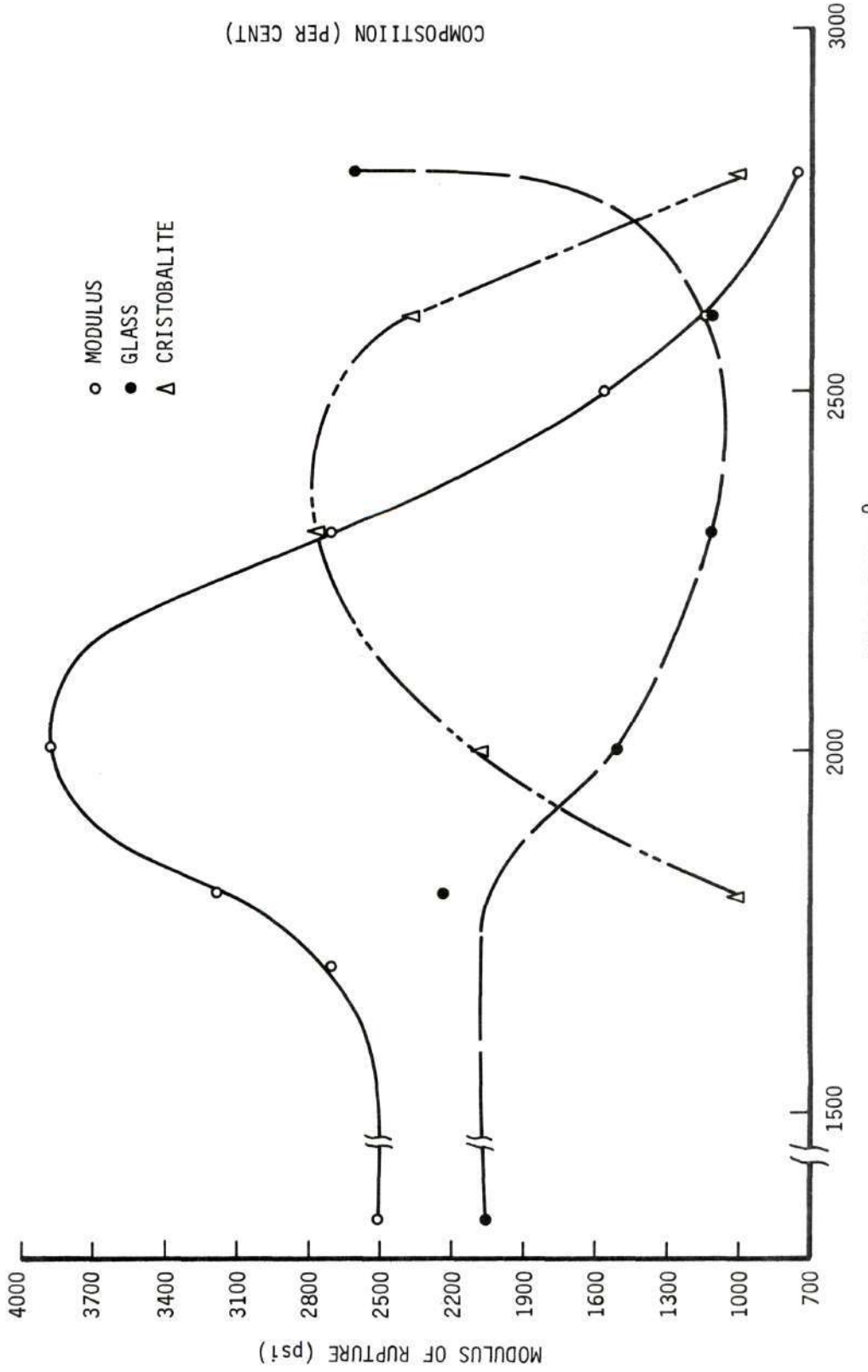

Figure 15. Composition and Strength Changes of Mullite Firebrick.

of cracks was made, cracks were observed at room temperature, Figure 14. The difference in thermal expansion coefficients of the phases fulfills the necessary conditions for closure at elevated temperatures.

The increase of alumina in the glassy phase will increase the shear force necessary for deformation. Also, the compositional change of the mullite indicates the presence of Al_2O_3 at the crystal - glass interface. This will increase the structural symmetry of the glass, and also serve as a nucleating agent for cristobalite.

The major causes of the strength increase at 2000°F are the increase of cristobalite and decrease of the glassy phase. The cristobalite present in the glass will increase the apparent viscosity of the refractory at a constant temperature. There is also the possibility of a cristobalite link between mullite grains originally separated by a thin film of glass. The loss of strength above 2300°F is controlled by the reduced viscosity and increased amount of the glassy phase.

High Alumina Refractory

Compositional and strength changes with temperature of the high alumina refractory are shown in Figure 16. The magnitude of the strength increase of the high alumina refractory (27 per cent) is substantially less than the mullite firebrick, and the compositional changes are correspondingly smaller. The decrease in the mullite and alumina found at 1800°F and above increases the amount of alumina and silica in the glass, and also the quantity of glass.

The causes of increased strength at 1800°F are compositional changes of the glassy phase; cohesive forces between particles; and closure of fissures. The alumina content of the glassy phase increases,

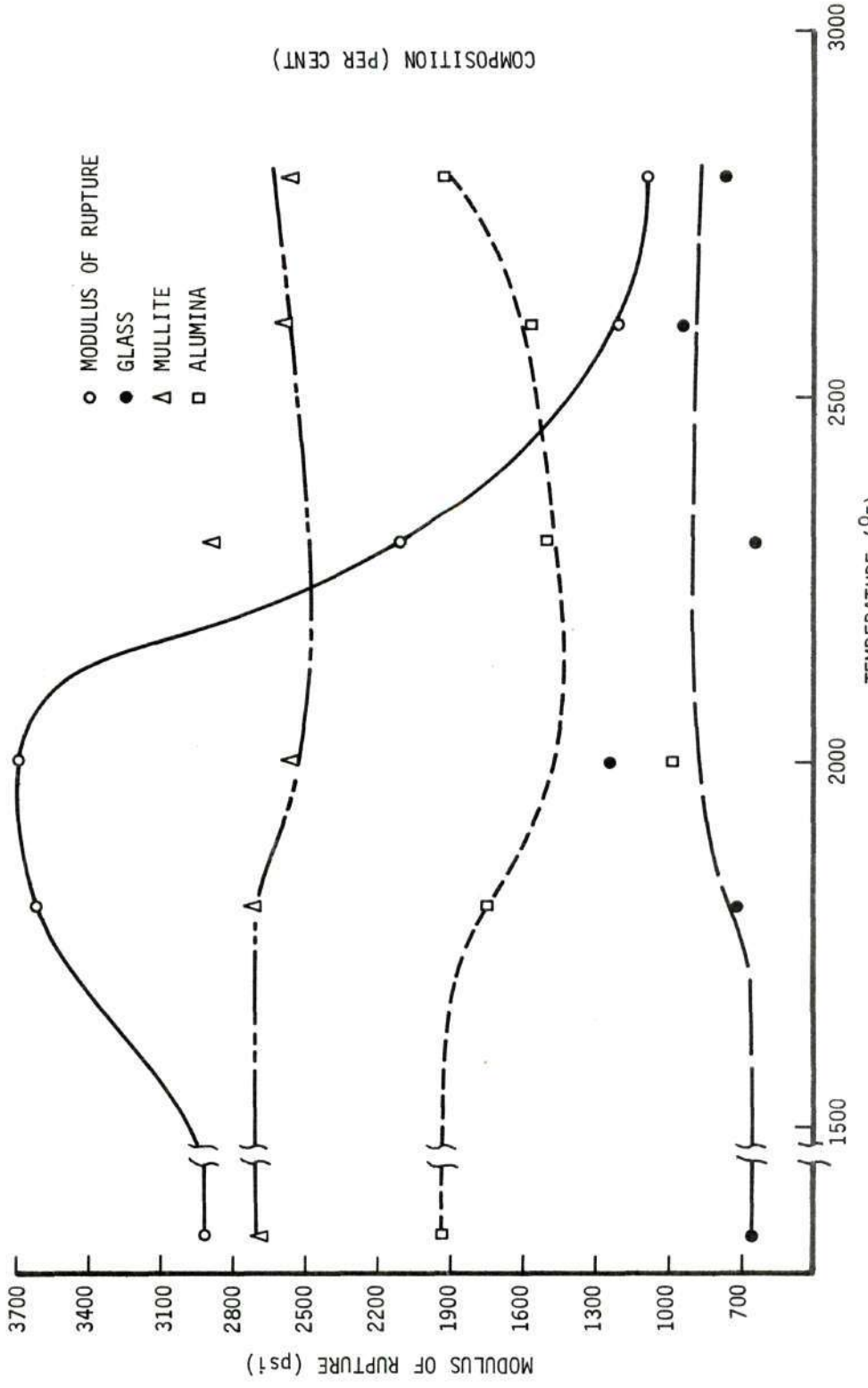

Figure 16. Composition and Strength Changes of High Alumina Refractory.

producing a more ordered glass structure. The increase of symmetry of the glass structure causes an increase in the force necessary to deform the refractory.

Some separation of crystalline and glassy phases was observed at room temperature. Closure of these fissures at elevated temperatures is probable because of differences in coefficients of thermal expansion. Evidence from strain measurements that the glass wets the alumina indicates the possibility of cohesive forces between the particles.

The strength increase at 2000°F is caused by further compositional changes in the glassy phase; stronger crystal - glass bond; and increase in direct bonding. The alumina content of the glassy phase continues to increase causing a decrease in the oxygen/cation ratio and, therefore, strengthening the glass at constant temperature.

The strain increase of the alumina corroborates a strong crystal-glass bond. This increased tension of the alumina indicates increased compressive stresses in the glassy phase. These compressive stresses serve as barriers for Griffith's flaws and increase the strength of the glass. The loss of strength above 2000°F is controlled by the reduced viscosity and increased amount of the glassy phase.

CHAPTER VI

CONCLUSIONS AND RECOMMENDATIONS

Conclusions

1. Compositional changes were measured at high temperatures and found to coincide with increases in strength in two alumino-silicate refractories.

2. The mullite firebrick exhibited a 54 per cent strength increase at 2000°F, the amount of cristobalite increase was seven per cent, and the corresponding decrease in glass content was 5.5 per cent. The increase of cristobalite in the glassy phase, cristobalite linking of mullite particles, and decrease of the glass content are the major causes of increased strength.

3. The amount of alumina and mullite change in the mullite firebrick was less than three per cent, and the mullite Al_2O_3/SiO_2 ratio decreased. The major role of these changes in strength increases was a nucleating agent for cristobalite.

4. In the high alumina refractory exhibiting a strength increase of 27 per cent, the changes in alumina, mullite, and glass were less than four per cent. Compositional changes do not appear to be as active or important in producing the strength increase as in the mullite firebrick. Additional mechanisms such as stress relief, closure of microcracks, and increase in direct bonding are operative.

5. Strain measurements of the alumina in both refractories indicate that stresses exist in the glass - alumina couple. This implies a

strong alumina - glass interface.

Recommendations

Additional studies of the compositional changes and physical properties of the glassy phase are needed for a better understanding of the strength of alumino-silicate refractories. In the mullite firebrick, the mechanism whereby the devitrification of a portion of the glassy phase increases the strength warrents further work.

Investigations of internal stresses, crystal - glass interface reactions, and comparison of macroscopic and microscopic thermal expansion coefficients of alumina - silicate refractories are necessary to substantiate present theories of increased strength at elevated temperatures.

APPENDIX A

X-RAY QUALITATIVE ANALYSIS

An important feature of this investigation is a knowledge of the crystalline phases present at each test temperature. In order to determine this, x-ray diffraction patterns were run on all specimens. The x-ray diffraction patterns of selected specimens are given in Tables 14 and 15. Experimental conditions for all qualitative x-ray diffraction work are given in Table 16.

Table 14. X-Ray Diffraction Pattern of Mullite Firebrick

A. Room Temperature

d-value (Å)	Relative Intensity	Line Identification	(h k l)
5.3938	49	Mullite	110
3.7745	5	Mullite	200
3.4834	70	Alumina	102
3.4406	72	Mullite	120
3.3920	100	Mullite	210
2.8887	18	Mullite	001
2.6961	38	Mullite	220
2.5474	44	Mullite	111
2.5474	100	Alumina	014
2.4274	13	Mullite	130
2.3809	40	Alumina	110
2.2934	15	Mullite	201
2.2097	56	Mullite	121
2.1219	21	Mullite	230
2.0855	100	Alumina	113
1.8881	5	Mullite	400
1.8433	8	Mullite	311
1.7415	30	Alumina	204
1.7202	5	Mullite	240
1.6909	10	Mullite	321
1.6014	90	Alumina	116
1.5801	5	Mullite	401
1.5256	31	Mullite	331
1.4629	5	Mullite	421
1.4449	13	Mullite	002
1.4058	40	Alumina	124
1.3748	30	Alumina	300
1.3362	8	Mullite	151
1.2776	8	Mullite	251
1.2638	8	Mullite	521
1.2394	20	Alumina	0.1.10

Table 14. X-Ray Diffraction Pattern of Mullite Firebrick

B. 1800°F

d-value (Å)	Relative Intensity	Line Identification	(h k l)
5.3905	46	Mullite	110
3.7745	5	Mullite	200
3.4834	70	Alumina	102
3.4280	70	Mullite	120
3.3896	100	Mullite	210
2.8887	16	Mullite	001
2.6937	38	Mullite	220
2.5474	38	Mullite	111
2.5474	100	Alumina	014
2.4274	11	Mullite	130
2.3809	40	Alumina	110
2.2947	11	Mullite	201
2.2097	57	Mullite	121
2.1219	19	Mullite	230
2.0855	100	Alumina	113
1.8881	8	Mullite	400
1.8433	5	Mullite	311
1.7415	40	Alumina	204
1.7143	5	Mullite	240
1.6937	8	Mullite	321
1.6014	90	Alumina	116
1.5801	5	Mullite	401
1.5256	30	Mullite	331
1.4617	5	Mullite	421
1.4444	14	Mullite	002
1.4048	40	Alumina	124
1.3739	30	Alumina	300
1.3365	8	Mullite	151
1.2784	8	Mullite	251
1.2638	8	Mullite	521
1.2394	20	Alumina	0.1.10

Table 14. X-Ray Diffraction Pattern of Mullite Firebrick

C. 2000°F

d-value (Å)	Relative Intensity	Line Identification	(h k l)
5.3905	47	Mullite	110
4.0826	100	Cristobalite	111
3.7745	5	Mullite	200
3.4834	78	Alumina	102
3.4280	68	Mullite	120
3.3896	100	Mullite	210
2.8868	18	Mullite	001
2.6937	37	Mullite	220
2.5474	39	Mullite	111
2.5474	100	Alumina	014
2.4306	13	Mullite	130
2.3809	33	Alumina	110
2.2934	13	Mullite	201
2.2087	55	Mullite	121
2.1213	18	Mullite	230
2.0863	100	Alumina	113
1.8863	5	Mullite	400
1.8426	8	Mullite	311
1.7415	44	Alumina	204
1.7143	5	Mullite	240
1.6937	11	Mullite	321
1.6019	89	Alumina	116
1.5801	5	Mullite	401
1.5256	29	Mullite	331
1.4617	5	Mullite	421
1.4444	11	Mullite	002
1.4058	44	Alumina	124
1.3748	22	Alumina	300
1.3362	8	Mullite	151
1.2784	8	Mullite	251
1.2638	8	Mullite	521
1.2394	22	Alumina	0.1.10

Table 14. X-Ray Diffraction Pattern of Mullite Firebrick

D. 2300°F

d-value (Å)	Relative Intensity	Line Identification	(h k l)
5.3841	49	Mullite	110
4.0826	100	Cristobalite	111
3.7745	5	Mullite	200
3.4807	57	Alumina	102
3.4280	73	Mullite	120
3.3896	100	Mullite	210
2.8868	19	Mullite	001
2.6961	38	Mullite	220
2.5474	32	Mullite	111
2.5474	100	Alumina	014
2.5145	13	Cristobalite	220
2.4274	14	Mullite	130
2.3809	21	Alumina	110
2.2934	14	Mullite	201
2.2071	62	Mullite	121
2.1213	19	Mullite	230
2.0863	100	Alumina	113
1.8863	5	Mullite	400
1.8433	8	Mullite	311
1.7415	43	Alumina	204
1.7143	5	Mullite	240
1.6909	11	Mullite	321
1.6023	86	Alumina	116
1.5789	5	Mullite	401
1.5256	27	Mullite	331
1.5109	14	Alumina	108
1.4617	5	Mullite	421
1.4434	11	Mullite	002
1.4048	29	Alumina	124
1.3748	29	Alumina	300
1.3362	8	Mullite	151
1.2784	8	Mullite	251
1.2638	8	Mullite	521
1.2394	14	Alumina	0.1.10

Table 14. X-Ray Diffraction Patterns of Mullite Firebrick

E. 2600°F

d-value (Å)	Relative Intensity	Line Identification	(h k l)
5.4004	46	Mullite	110
4.0826	100	Cristobalite	111
3.7773	6	Mullite	200
3.4834	88	Alumina	102
3.4406	69	Mullite	120
3.3873	100	Mullite	210
2.8868	20	Mullite	001
2.6961	41	Mullite	220
2.5474	48	Mullite	111
2.5474	100	Alumina	014
2.5145	17	Cristobalite	220
2.4274	14	Mullite	130
2.3809	69	Alumina	110
2.2934	14	Mullite	201
2.2087	55	Mullite	121
2.1219	19	Mullite	230
2.0878	100	Alumina	113
1.8881	6	Mullite	400
1.8426	8	Mullite	311
1.7409	56	Alumina	204
1.7143	6	Mullite	240
1.6952	11	Mullite	321
1.6023	88	Alumina	116
1.5801	5	Mullite	401
1.5256	29	Mullite	331
1.5121	13	Alumina	108
1.4617	4	Mullite	421
1.4444	13	Mullite	002
1.4257	3	Mullite	250
1.4058	50	Alumina	124
1.3748	50	Alumina	300
1.3479	3	Mullite	440
1.3370	9	Mullite	151
1.2784	8	Mullite	251
1.2638	8	Mullite	521
1.2397	44	Alumina	0.1.10

Table 14. X-Ray Diffraction Pattern of Mullite Firebrick

F. 2800°F

d-value (Å)	Relative Intensity	Line Identification	(h k l)
5.4004	48	Mullite	110
3.7745	6	Mullite	200
3.4834	78	Alumina	102
3.4406	73	Mullite	120
3.3920	100	Mullite	210
2.8887	18	Mullite	001
2.6961	40	Mullite	220
2.5474	38	Mullite	111
2.5474	100	Alumina	014
2.4283	13	Mullite	130
2.3809	44	Alumina	110
2.2934	16	Mullite	201
2.2097	58	Mullite	121
2.1228	21	Mullite	230
2.0878	100	Alumina	113
1.8881	7	Mullite	400
1.8433	8	Mullite	311
1.7409	44	Alumina	204
1.7143	6	Mullite	240
1.6952	11	Mullite	321
1.6027	39	Alumina	116
1.5801	4	Mullite	401
1.5256	31	Mullite	331
1.4609	7	Mullite	421
1.4444	13	Mullite	002
1.4357	3	Mullite	250
1.4058	39	Alumina	124
1.3757	35	Alumina	300
1.3470	3	Mullite	440
1.3370	8	Mullite	151
1.2784	8	Mullite	251
1.2638	7	Mullite	521
1.2400	22	Alumina	0.1.10

Table 15. X-Ray Diffraction Pattern of High Alumina Refractory

A. Room Temperature

d-value (Å)	Relative Intensity	Line Identification	(h k l)
5.3971	54	Mullite	110
3.4834	72	Alumina	102
3.4406	69	Mullite	120
3.3984	100	Mullite	210
2.8914	15	Mullite	001
2.7001	38	Mullite	220
2.5523	31	Mullite	111
2.5523	100	Alumina	014
2.4306	8	Mullite	130
2.3809	40	Alumina	110
2.2962	16	Mullite	201
2.2097	54	Mullite	121
2.1228	23	Mullite	230
2.0863	100	Alumina	113
1.7391	46	Alumina	204
1.6023	74	Alumina	116
1.5469	2	Alumina	411
1.5278	23	Mullite	331
1.5117	9	Alumina	108
1.4444	8	Mullite	002
1.4048	33	Alumina	124
1.3744	36	Alumina	300
1.3362	8	Mullite	151
1.2394	12	Alumina	0.1.10

Table 15. X-Ray Diffraction Pattern of High Alumina Refractory

B. 1800°F

d-value (Å)	Relative Intensity	Line Identification	(h k l)
5.4004	55	Mullite	110
3.4807	69	Alumina	102
3.4406	73	Mullite	120
3.3984	100	Mullite	210
2.8914	18	Mullite	001
2.6961	46	Mullite	220
2.5509	73	Mullite	111
2.5509	100	Alumina	014
2.4306	18	Mullite	130
2.3791	42	Alumina	110
2.2990	18	Mullite	201
2.2097	55	Mullite	121
2.1228	27	Mullite	230
2.0863	100	Alumina	113
1.7430	37	Alumina	204
1.6019	67	Alumina	116
1.5278	27	Mullite	331
1.5109	4	Alumina	108
1.4451	9	Mullite	002
1.4048	27	Alumina	124
1.3744	37	Alumina	300
1.3362	9	Mullite	151
1.2394	12	Alumina	0.1.10

Table 15. X-Ray Diffraction Pattern of High Alumina Refractory

C. 2000°F

d-value (Å)	Relative Intensity	Line Identification	(h k l)
5.4004	62	Mullite	110
3.4834	67	Alumina	102
3.4406	69	Mullite	120
3.3984	100	Mullite	210
2.8868	15	Mullite	001
2.6977	38	Mullite	220
2.7001	95	Alumina	014
2.4306	15	Mullite	130
2.3803	40	Alumina	110
2.2986	15	Mullite	201
2.2097	46	Mullite	121
2.1252	23	Mullite	230
2.0855	100	Alumina	113
1.7406	35	Alumina	204
1.6981	8	Mullite	321
1.6023	75	Alumina	116
1.5471	3	Alumina	411
1.5272	23	Mullite	331
1.5109	7	Alumina	108
1.4449	8	Mullite	002
1.4048	25	Alumina	124
1.3741	43	Alumina	300
1.3362	8	Mullite	151
1.2394	8	Alumina	0.1.10

Table 15. X-Ray Diffraction Pattern of High Alumina Refractory

D. 2300°F

d-value (Å)	Relative Intensity	Line Identification	(h k l)
5.4070	62	Mullite	110
3.4834	71	Alumina	102
3.4406	77	Mullite	120
3.3984	100	Mullite	210
2.8914	15	Mullite	001
2.6985	38	Mullite	220
2.7001	23	Mullite	111
2.7001	100	Alumina	014
2.4306	15	Mullite	130
2.3809	36	Alumina	110
2.2962	15	Mullite	201
2.2097	54	Mullite	121
2.1228	23	Mullite	230
2.0863	100	Alumina	113
1.7406	36	Alumina	204
1.6996	15	Mullite	321
1.6019	66	Alumina	116
1.5475	2	Alumina	411
1.5278	31	Mullite	331
1.5121	7	Alumina	108
1.4434	15	Mullite	002
1.4048	25	Alumina	124
1.3744	38	Alumina	300
1.3362	15	Mullite	151
1.2394	13	Alumina	0.1.10

Table 15. X-Ray Diffraction Pattern of High Alumina Refractory

E. 2600°F

d-value (Å)	Relative Intensity	Line Identification	(h k l)
5.4004	62	Mullite	110
3.4807	66	Alumina	102
3.4406	69	Mullite	120
3.3984	100	Mullite	210
2.8868	15	Mullite	001
2.6985	38	Mullite	220
2.5509	99	Mullite	111
2.5509	100	Alumina	014
2.4306	15	Mullite	130
2.3797	39	Alumina	110
2.2990	15	Mullite	201
2.2097	54	Mullite	121
2.1252	23	Mullite	230
2.0855	100	Alumina	113
1.7430	41	Alumina	204
1.6990	8	Mullite	321
1.6019	85	Alumina	116
1.5475	4	Alumina	411
1.5278	23	Mullite	331
1.5109	3	Alumina	108
1.4048	29	Alumina	124
1.3739	41	Alumina	300
1.3370	15	Mullite	151
1.2394	14	Alumina	0.1.10

Table 15. X-Ray Diffraction Pattern of High Alumina Refractory

F. 2800°F

d-value (Å)	Relative Intensity	Line Identification	(h k l)
5.4004	58	Mullite	110
3.4834	71	Alumina	102
3.4332	75	Mullite	120
3.3984	100	Mullite	210
2.8868	17	Mullite	001
2.7001	42	Mullite	220
2.5509	42	Mullite	111
2.5509	100	Alumina	014
2.4306	17	Mullite	130
2.3809	36	Alumina	110
2.2962	17	Mullite	201
2.2097	50	Mullite	121
2.1228	25	Mullite	230
2.0863	100	Alumina	113
1.7406	42	Alumina	204
1.6996	8	Mullite	321
1.6027	64	Alumina	116
1.5475	2	Alumina	411
1.5278	25	Mullite	331
1.5109	5	Alumina	108
1.4048	27	Alumina	124
1.3739	38	Alumina	300
1.3370	8	Mullite	151
1.2394	13	Alumina	0.1.10

Table 16. Experimental Conditions for Qualitative X-Ray Diffraction Analysis

Factor	Setting
Killivolts	40Kv
Milliamperes	24ma
Time Constant	1
Scale Factor	1×10^3
Chart Speed	1/2 inch/minute
Scan Speed	1° 2θ/minute
Pulse Height Analyser	95% Transmission
Radiation	Copper K_α
Filter	Nickel
Divergence Slit	1°
Receiving Slit	0.003 in.
Scatter Split	1°
Recorder Span	10Mv

APPENDIX B

X-RAY QUANTITATIVE ANALYSIS

Powder x-ray diffraction analysis is seemingly the ideal technique for crystalline-mixture analysis, since each component of the mixture produces its characteristic pattern independently of the others. The intensity of each component's pattern is proportional to the amount present except for an absorption correction. With the use of an internal standard, no correction of the intensities because of absorption need be made.

Calcium fluoride, fluorite, was chosen as the internal standard. The standard sample data for alumina and mullite is given in Table 17. Table 18 gives the standard sample data for cristobalite. The experimental conditions for the x-ray quantitative analysis of alumina, mullite, and cristobalite are given in Table 19.

Table 17. Standard Sample Data for Alumina and Mullite Calibration Curves

Weight in grams of Alumina	Mullite	Fluorite	Per Cent Alumina	Per Cent Mullite	Peak Area $\frac{\text{Alumina}}{\text{Peak Area } CaF_2}$	Peak Area $\frac{\text{Mullite}}{\text{Peak Area } CaF_2}$
0.000	4.000	2.000	0.0	100.0	0.000	0.299
0.200	3.800	2.000	5.0	95.0	0.015	0.270
0.400	3.600	2.000	10.0	90.0	0.033	0.241
0.600	3.400	2.000	15.0	85.0	0.035	0.240
0.800	3.200	2.000	20.0	80.0	0.046	0.228
1.000	3.000	2.000	25.0	75.0	0.061	0.237
1.200	2.800	2.000	30.0	70.0	0.081	0.174
1.400	2.600	2.000	35.0	65.0	0.082	0.180
1.600	2.400	2.000	40.0	60.0	0.083	0.157
1.800	2.200	2.000	45.0	55.0	0.094	0.163
2.000	2.000	2.000	50.0	50.0	0.121	0.150
2.200	1.800	2.000	55.0	45.0	0.131	0.135
2.400	1.600	2.000	60.0	40.0	0.115	0.101
2.800	1.200	2.000	70.0	30.0	0.147	0.063
3.200	0.800	2.000	80.0	20.0	0.181	0.047
3.600	0.400	2.000	90.0	10.0	0.219	0.024
4.000	0.000	2.000	100.0	0.0	0.231	0.000

Table 18. Standard Sample Data for Cristobalite Calibration Curve

Weight in grams of Cristobalite	Alumina	Fluorite	Per Cent Cristobalite	Peak Area Cristobalite / Peak Area Fluorite
0.200	3.800	2.000	5.0	0.164
0.400	3.600	2.000	10.0	0.289
0.600	3.400	2.000	15.0	0.470
0.800	3.200	2.000	20.0	0.607
1.000	3.000	2.000	25.0	0.805
1.200	2.800	2.000	30.0	0.928
1.400	2.600	2.000	35.0	1.062
1.600	2.400	2.000	40.9	1.226
1.800	2.200	2.000	45.0	1.353
2.000	2.000	2.000	50.0	1.487

Table 19. Experimental Conditions for X-Ray Quantitative Analysis

Factor	Alumina and Mullite	Cristobalite
Killivolts	40 Kv	40 Kv
Milliamperes	24 ma	24 ma
Time Constant	4	4
Scale Factor	$1x10^3$	$5x10^2$ 0% - 20% $1x10^3$ 25% - 50%
Chart Speed	1/2 inch/minute	1/2 inch/minute
Scan Speed	1/4° 2θ/minute	1/4° 2θ/minute
Pulse Height Analyser	95% Transmission	95% Transmission
Radiation	Copper K_α	Copper K_α
Filter	Nickel	Nickel
Divergence Slit	1°	1°
Receiving Slit	0.003 inches	0.003 inches
Scatter Slit	1°	1°
Recorder Span	10 MV	10 MV

APPENDIX C

LINEAR REGRESSION

The linear regression procedure is a method of obtaining a least squares fit to data that show a linear trend. As an example of this calculation, the data for the alumina calibration curve will be used. The example given is for the special case of the functional relationship where errors of measurement affect only one variable (Y) and the intercept is known to be equal to zero. Data calculated for the alumina standard are given in Table 17.

The slope of the regression line is b, where:

$$b = \frac{\Sigma XY}{\Sigma X^2}$$

Thus the equation for the straight line with the intercept equal to zero has the familiar form:

$$Y = bX$$

Where:

X = ratio of peak area of alumina to peak area of calcium fluoride

Y = ratio of grams of alumina to grams of calcium fluoride

Calculated values are given in Table 20.

Table 20. Calculation of the Regression Equation

X denotes $\frac{A_a}{A_S}$	Y denotes $\frac{\text{grams } Al_2O_3}{\text{grams } CaF_2}$
$\Sigma X = 1.6697$	$\Sigma Y = 14.6000$
$\bar{X} = 0.1044$	$\bar{Y} = 0.9130$
$n = 16$	
$\Sigma XY = 2.0749$	$\frac{(\Sigma XY)^2}{\Sigma X^2} = 18.1501$
$\Sigma X^2 = 0.2372$	
$\Sigma Y^2 = 18.2600$	
$b = \frac{\Sigma XY}{\Sigma X^2} = 8.7475$	$(n-1)\, S_Y^2 = 0.1099$
	$S_Y^2 = 0.0073$
	$S_Y = 0.0854$

Estimate of variance of the slope:

$$S_b^2 = \frac{S_Y^2}{\Sigma X^2} = 0.0308$$

$$S_b = 0.1755$$

Equation of the Line:

$$Y = 8.7475\ X$$

APPENDIX D

REPRODUCIBILITY OF QUANTITATIVE X-RAY DIFFRACTION DATA

The purpose of this section is to give the reproducibility of quantitative x-ray diffraction measurements that was obtained with a constant weight per cent of mullite, tabular alumina, and cristobalite. Measurements on a given specimen which was not repacked between runs were quite reproducible. It appears, therefore, that the major cause of differences were due to variations in the packing of the specimens. It should be emphasized that the deviations given are caused only by experimental techniques. The errors reported are per cent standard deviation from the mean value.

In the case of mullite and alumina the reproducibility is calculated from thirty measurements of a room temperature specimen. The per cent standard deviations found for the mullite and alumina content were three and six per cent, respectively. The reproducibility of the cristobalite content is based on twenty measurements of specimens fired to 2000°F. A deviation of eight per cent was found.

APPENDIX E

QUANTITATIVE X-RAY DIFFRACTION DATA

The following data were collected from quantitative x-ray diffraction of the specimens. The values given are the average of two or more determinations on each specimen. All areas are in square inches.

Table 21. Quantitative X-Ray Diffraction Data for Mullite Firebrick

A. Room Temperature

Specimen Number	Integrated Mullite	Area of Reflection For CaF_2	Al_2O_3	$\frac{Am}{ACaF_2}$	$\frac{Aa}{ACaF_2}$	Weight Per cent of Mullite	Al_2O_3	Glass
R-1-Q-1	0.62	3.98	0.15	0.1558	0.0377	54.0	16.5	29.5
R-1-Q-2	0.65	4.06	0.12	0.1600	0.0296	55.6	13.0	31.4
R-1-Q-3	0.62	4.07	0.19	0.1523	0.0467	53.0	20.3	26.7
R-1-Q-4	0.58	4.12	0.19	0.1408	0.0461	49.0	20.0	31.0
R-1-Q-5	0.54	4.10	0.17	0.1317	0.0415	45.9	18.0	36.1

B. 1800°F

Specimen Number	Integrated Mullite	Area of Reflection For CaF_2	Al_2O_3	$\frac{Am}{ACaF_2}$	$\frac{Aa}{ACaF_2}$	Weight Per cent of Mullite	Al_2O_3	Glass
1-Q-1	0.55	4.04	0.12	0.1361	0.0297	45.6	12.9	41.5
1-Q-2	0.63	3.75	0.11	0.1680	0.0293	58.5	12.7	28.8
1-Q-3	0.59	3.93	0.15	0.1501	0.0382	52.1	16.6	31.3
1-Q-4	0.57	3.93	0.11	0.1450	0.0280	50.4	12.1	37.5
1-Q-5	0.65	4.21	0.14	0.1544	0.0333	53.7	14.5	31.8

Table 21. Quantitative X-Ray Diffraction Data for Mullite Firebrick

C. Room Temperature

Specimen Number	Integrated Mullite	Area of Reflection for CaF_2	Area of Reflection for Al_2O_3	$\frac{Am}{ACaF_2}$	$\frac{Aa}{ACaF_2}$	Weight Per Cent of Mullite	Weight Per Cent of Al_2O_3	Weight Per Cent of Glass
R-1-Q-6	0.59	3.95	0.13	0.1494	0.0329	52.0	14.5	33.5
R-1-Q-7	0.56	3.96	0.15	0.1414	0.0379	49.2	16.5	34.3
R-1-Q-8	0.55	4.15	0.14	0.1323	0.0337	46.0	14.7	39.3
R-1-Q-9	0.52	4.08	0.19	0.1275	0.0466	44.3	20.7	35.0
R-1-Q-10	0.56	3.88	0.14	0.1443	0.0361	50.0	15.6	34.4
R-1-Q-11	0.59	3.97	0.11	0.1486	0.0277	51.7	12.2	36.1
R-1-Q-12	0.65	4.55	0.18	0.1429	0.0396	49.8	12.2	38.0
R-1-Q-13	0.68	4.55	0.20	0.1495	0.0440	52.0	19.0	29.0
R-1-Q-14	0.70	4.73	0.13	0.1480	0.0275	51.5	17.0	31.5
R-1-Q-15	0.64	4.30	0.15	0.1488	0.0349	51.7	14.8	33.5

Table 21. Quantitative X-Ray Diffraction Data for Mullite Firebrick

D. 2000°F

Specimen Number	Integrated Area of Reflection for Mullite	CaF_2	Al_2O_3	Cristobalite	$\frac{Am}{ACaF_2}$	$\frac{Aa}{ACaF_2}$	$\frac{ASiO_2}{ACaF_2}$	Weight per cent of Mullite	Al_2O_3	Cristobalite	Glass
1-Q-6	0.58	4.47	0.15	0.75	0.1303	0.0342	0.1687	45.1	14.8	6.0	34.1
1-Q-7	0.63	4.40	0.15	0.84	0.1432	0.0341	0.1909	49.8	15.2	6.6	28.4
1-Q-8	0.62	4.40	0.15	0.82	0.1409	0.0341	0.1864	49.0	15.2	6.5	29.3
1-Q-9	0.62	4.27	0.21	0.87	0.1452	0.0492	0.2037	50.5	21.3	7.3	20.9
1-Q-10	0.57	4.26	0.11	0.86	0.1338	0.0258	0.2019	46.5	11.3	7.1	35.1
1-Q-11	0.63	4.50	0.16	0.98	0.1400	0.0356	0.2178	48.5	15.5	7.8	28.2
1-Q-12	0.65	4.59	0.20	0.94	0.1416	0.0436	0.2048	49.3	18.9	7.3	24.5
1-Q-13	0.67	4.49	0.18	1.09	0.1492	0.0400	0.2428	51.9	17.4	8.4	22.3
1-Q-14	0.59	3.98	0.22	0.83	0.1482	0.0553	0.2085	51.5	24.0	7.5	17.0
1-Q-15	0.61	4.07	0.13	0.97	0.1499	0.0319	0.2383	52.1	14.0	8.7	25.2

Table 21. Quantitative X-Ray Diffraction Data for Mullite Firebrick

E. Room Temperature

Specimen Number	Integrated Area of Reflection for Mullite	CaF_2	Al_2O_3	$\frac{Am}{ACaF_2}$	$\frac{Aa}{ACaF_2}$	Weight Per Cent of Mullite	Al_2O_3	Glass
R-1-Q-16	0.62	4.10	0.13	0.1512	0.0317	52.5	13.8	33.7
R-1-Q-17	0.66	4.47	0.15	0.1477	0.0336	51.4	14.5	34.1
R-1-Q-18	0.60	3.92	0.15	0.1531	0.0383	53.3	16.7	30.0
R-1-Q-19	0.62	4.43	0.12	0.1400	0.0271	48.5	11.8	39.7
R-1-Q-20	0.63	4.23	0.15	0.1489	0.0355	51.7	15.4	32.9

F. 2300°F

Specimen Number	Integrated Area of Reflection for Mullite	CaF_2	Al_2O_3	Cristobalite	$\frac{Am}{ACaF_2}$	$\frac{Aa}{ACaF_2}$	$\frac{ASiO_2}{ACaF_2}$	Mullite	Al_2O_3	Cristobalite	Glass
1-Q-16	0.60	4.27	0.17	1.53	0.1405	0.0398	0.3583	48.5	17.3	12.3	21.9
1-Q-17	0.63	4.65	0.14	1.57	0.1355	0.0301	0.3376	47.0	13.0	11.5	28.5
1-Q-18	0.67	4.64	0.22	1.62	0.1444	0.0474	0.3491	50.0	20.5	11.8	17.7
1-Q-19	0.61	4.56	0.13	1.64	0.1338	0.0285	0.3596	46.5	12.3	12.3	28.9
1-Q-20	0.63	4.57	0.13	1.56	0.1379	0.0284	0.3414	47.8	12.3	11.7	28.2

Table 21. Quantitative X-Ray Diffraction Data for Mullite Firebrick

G. Room Temperature

Specimen Number	Integrated Area of Reflection for Mullite	CaF_2	Al_2O_3	$\frac{Am}{A_{CaF_2}}$	$\frac{Aa}{A_{CaF_2}}$	Weight Per cent of Mullite	Al_2O_3	Glass
R-1-Q-21	0.65	4.52	0.15	0.1438	0.0332	49.9	14.5	35.6
R-1-Q-22	0.60	4.43	0.18	0.1354	0.0406	47.0	17.7	35.3
R-1-Q-23	0.68	4.41	0.15	0.1542	0.0340	53.6	14.8	31.6
R-1-Q-24	0.61	4.06	0.17	0.1502	0.0419	52.1	18.2	29.7
R-1-Q-25	0.59	3.94	0.16	0.1497	0.0406	52.0	17.7	30.3

H. 2600°F

Specimen Number	Integrated Area of Reflection for Mullite	CaF_2	Al_2O_3	Cristobalite	$\frac{Am}{A_{CaF_2}}$	$\frac{Aa}{A_{CaF_2}}$	$\frac{ASiO_2}{A_{CaF_2}}$	Weight Per cent of Mullite	Al_2O_3	Cristobalite	Glass
1-Q-21	0.66	4.60	0.18	1.00	0.1435	0.0391	0.2174	49.8	17.5	7.7	25.0
1-Q-22	0.61	4.56	0.16	0.91	0.1338	0.0351	0.1996	46.5	15.2	7.0	31.3
1-Q-23	0.67	4.38	0.16	1.40	0.1530	0.0365	0.3196	53.2	16.0	11.0	19.8
1-Q-24	0.53	4.39	0.14	1.12	0.1207	0.0319	0.2551	42.0	14.0	8.9	35.1
1-Q-25	0.58	4.12	0.12	0.98	0.1408	0.0291	0.2379	48.9	12.1	8.3	30.7

Table 21. Quantitative X-Ray Diffraction Data for Mullite Firebrick

I. Room Temperature

Specimen Number	Integrated Area of Reflection for Mullite	CaF_2	Al_2O_3	$\frac{Am}{A_{CaF_2}}$	$\frac{Aa}{A_{CaF_2}}$	Weight Per cent of Mullite	Al_2O_3	Glass
R-1-Q-26	0.61	3.95	0.18	0.1544	0.0456	53.7	19.8	26.5
R-1-Q-27	0.59	4.11	0.15	0.1436	0.0365	49.9	16.0	34.1
R-1-Q-28	0.60	4.12	0.17	0.1456	0.0413	50.6	18.0	31.4
R-1-Q-29	0.60	3.92	0.15	0.1531	0.0383	53.4	16.6	30.0
R-1-Q-30	0.61	4.19	0.15	0.1456	0.0358	50.6	15.5	33.9

J. 2800°F

Specimen Number	Integrated Area of Reflection for Mullite	CaF_2	Al_2O_3	$\frac{Am}{A_{CaF_2}}$	$\frac{Aa}{A_{CaF_2}}$	Weight Per cent of Mullite	Al_2O_3	Glass
1-Q-26	0.51	4.13	0.12	0.1235	0.0291	43.0	12.7	44.3
1-Q-27	0.61	4.09	0.17	0.1492	0.0416	51.8	18.0	30.2
1-Q-28	0.55	3.95	0.14	0.1392	0.0354	48.3	15.5	36.2
1-Q-29	0.56	4.10	0.14	0.1366	0.0341	47.5	15.0	37.5
1-Q-30	0.59	4.12	0.20	0.1432	0.0485	49.8	21.0	29.2

Table 21. Quantitative X-Ray Diffraction Data for Mullite Firebrick

K. Room Temperature

Specimen Number	Integrated Area of Reflection for Mullite	CaF_2	Al_2O_3	$\frac{Am}{A_{CaF_2}}$	$\frac{Aa}{A_{CaF_2}}$	Weight Per Cent of Mullite	Al_2O_3	Glass
R-1-C-6	0.70	4.41	0.17	0.1587	0.0385	55.2	16.7	28.1
R-1-C-7	0.58	4.25	0.16	0.1365	0.0376	47.5	16.4	36.1
R-1-C-16	0.62	4.07	0.20	0.1523	0.0491	53.0	21.4	25.6
R-1-C-17	0.65	4.17	0.15	0.1559	0.0360	54.3	15.5	30.2

L. Cooled Slowly

Temperature °F	Specimen Number	Integrated Area of Reflection for Mullite	CaF_2	Al_2O_3	Cristobalite	$\frac{Am}{A_{CaF_2}}$	$\frac{Aa}{A_{CaF_2}}$	$\frac{ASiO_2}{A_{CaF_2}}$	Weight Per cent of Mullite	Al_2O_3	Cristobalite	Glass
2000	1-C-6	0.64	4.55	0.20	1.04	0.1407	0.0440	0.2286	48.8	19.1	7.9	24.2
2000	1-C-7	0.58	4.12	0.18	0.88	0.1408	0.0437	0.2136	48.8	19.1	7.5	24.6
2300	1-C-16	0.61	4.25	0.17	1.64	0.1435	0.0400	0.3859	50.0	17.4	13.2	19.4
2300	1-C-17	0.60	4.36	0.16	1.77	0.1376	0.0367	0.4060	47.7	16.0	13.8	22.5

Table 22. Quantitative X-Ray Diffraction Data for High Alumina Refractory

A. Room Temperature

Specimen Number	Integrated Area of Reflection for Mullite	CaF_2	Al_2O_3	$\frac{Am}{A_{CaF_2}}$	$\frac{Aa}{A_{CaF_2}}$	Weight Per cent of Mullite	Al_2O_3	Glass
R-3-Q-1	0.20	4.75	0.85	0.0421	0.1789	14.5	78.5	7.0
R-3-Q-2	0.20	4.26	0.76	0.0469	0.1784	16.3	78.4	5.3
R-3-Q-3	0.20	4.35	0.77	0.0460	0.1770	15.8	77.3	6.9
R-3-Q-4	0.21	4.26	0.75	0.0493	0.1761	17.0	76.7	6.3
R-3-Q-5	0.21	4.44	0.80	0.0473	0.1802	16.9	78.5	4.6

B. 1800°F

Specimen Number	Integrated Area of Reflection for Mullite	CaF_2	Al_2O_3	$\frac{Am}{A_{CaF_2}}$	$\frac{Aa}{A_{CaF_2}}$	Weight Per cent of Mullite	Al_2O_3	Glass
3-Q-1	0.26	4.75	0.87	0.0547	0.1832	18.9	79.8	1.3
3-Q-2	0.22	4.50	0.86	0.0489	0.1911	16.8	83.2	0.0
3-Q-3	0.23	4.67	0.81	0.0493	0.1734	17.0	75.4	7.6
3-Q-4	0.23	4.61	0.79	0.0499	0.1714	17.3	74.8	7.9
3-Q-5	0.20	4.73	0.86	0.0423	0.1818	14.5	79.2	6.3

Table 22. Quantitative X-Ray Diffraction Data for High Alumina Refractory

C. Room Temperature

Specimen Number	Integrated Area of Reflection for Mullite	CaF_2	Al_2O_3	$\frac{Am}{A_{CaF_2}}$	$\frac{Aa}{A_{CaF_2}}$	Weight Per cent of Mullite	Al_2O_3	Glass
R-3-Q-6	0.18	4.22	0.88	0.0427	0.2085	14.9	91.0	---
R-3-Q-7	0.23	4.23	0.72	0.0544	0.1702	18.8	74.1	7.1
R-3-Q-8	0.21	4.16	0.94	0.0505	0.2260	17.4	98.4	---
R-3-Q-9	0.22	4.01	0.64	0.0548	0.1596	19.6	69.5	10.9
R-3-Q-10	0.21	4.22	0.65	0.0498	0.1540	17.2	67.2	15.6
R-3-Q-11	0.20	4.10	0.65	0.0488	0.1585	16.8	69.0	14.2
R-3-Q-12	0.20	4.07	0.74	0.0491	0.1818	17.0	79.3	3.7
R-3-Q-13	0.20	4.19	0.70	0.0477	0.1671	16.4	72.7	10.9
R-3-Q-14	0.22	4.26	0.84	0.0516	0.1972	17.7	86.0	---
R-3-Q-15	0.21	4.36	0.63	0.0482	0.1445	16.5	63.0	20.5

Table 22. Quantitative X-Ray Diffraction Data for High Alumina Refractory

D. 2000°F

Specimen Number	Integrated Area of Reflection for Mullite	CaF_2	Al_2O_3	$\frac{Am}{A_{CaF_2}}$	$\frac{Aa}{A_{CaF_2}}$	Weight Per cent of Mullite	Al_2O_3	Glass
3-Q-6	0.21	4.19	0.71	0.0501	0.1695	17.2	73.8	9.0
3-Q-7	0.21	4.41	0.79	0.0476	0.1791	16.3	78.0	5.8
3-Q-8	0.25	4.34	0.83	0.0576	0.1912	19.9	83.4	---
3-Q-9	0.19	4.37	0.73	0.0435	0.1670	15.0	72.8	12.2
3-Q-10	0.21	4.18	0.66	0.0502	0.1579	17.2	68.9	13.9
3-Q-11	0.20	4.42	0.75	0.0452	0.1697	15.5	73.8	10.7
3-Q-12	0.20	4.37	0.80	0.0458	0.1831	15.8	79.9	4.3
3-Q-13	0.19	4.21	0.81	0.0451	0.1924	15.5	84.0	0.5
3-Q-14	0.18	4.88	0.78	0.0369	0.1598	12.8	69.6	17.6
3-Q-15	0.21	4.69	0.83	0.0448	0.1770	15.4	77.2	7.4

Table 22. Quantitative X-Ray Diffraction Data for High Alumina Refractory

E. Room Temperature

Specimen Number	Integrated Area of Reflection for Mullite	CaF_2	Al_2O_3	$\frac{Am}{A_{CaF_2}}$	$\frac{Aa}{A_{CaF_2}}$	Weight Per cent of Mullite	Al_2O_3	Glass
R-3-Q-16	0.23	4.56	0.78	0.0504	0.1711	17.4	74.5	8.1
R-3-Q-17	0.22	4.76	0.90	0.0462	0.1891	15.9	82.4	1.7
R-3-Q-18	0.20	4.58	0.89	0.0437	0.1943	15.0	84.7	0.3
R-3-Q-19	0.20	4.42	0.80	0.0452	0.1810	15.5	78.9	5.6
R-3-Q-20	0.19	4.21	0.92	0.0451	0.2185	15.5	95.0	---

F. 2300°F

Specimen Number	Integrated Area of Reflection for Mullite	CaF_2	Al_2O_3	$\frac{Am}{A_{CaF_2}}$	$\frac{Aa}{A_{CaF_2}}$	Weight Per cent of Mullite	Al_2O_3	Glass
3-Q-16	0.23	4.59	0.70	0.0501	0.1525	17.9	66.5	15.6
3-Q-17	0.28	4.68	0.85	0.0598	0.1816	20.7	79.1	0.2
3-Q-18	0.23	4.69	0.88	0.0490	0.1876	17.4	81.8	0.8
3-Q-19	0.25	4.49	0.77	0.0558	0.1719	20.0	74.6	5.4
3-Q-20	0.21	4.54	0.78	0.0463	0.1718	15.9	74.4	9.7

Table 22. Quantitative X-Ray Diffraction Data for High Alumina Refractory

G. Room Temperature

Specimen Number	Integrated Area of Reflection for Mullite	CaF_2	Al_2O_3	$\frac{Am}{A_{CaF_2}}$	$\frac{Aa}{A_{CaF_2}}$	Weight Per cent of Mullite	Al_2O_3	Glass
R-3-Q-21	0.24	4.80	0.80	0.0500	0.1667	17.2	72.7	9.1
R-3-Q-22	0.21	4.68	0.89	0.0449	0.1902	15.5	82.9	1.6
R-3-Q-23	0.23	4.59	0.86	0.0501	0.1874	17.2	81.7	1.1
R-3-Q-24	0.23	4.65	0.87	0.0495	0.1871	17.0	81.6	1.4
R-3-Q-25	0.21	4.44	0.84	0.0473	0.1892	16.8	82.4	0.8

H. 2600°F

Specimen Number	Integrated Area of Reflection for Mullite	CaF_2	Al_2O_3	$\frac{Am}{A_{CaF_2}}$	$\frac{Aa}{A_{CaF_2}}$	Weight Per cent of Mullite	Al_2O_3	Glass
3-Q-21	0.22	4.73	0.99	0.0465	0.2093	16.0	91.2	---
3-Q-22	0.23	4.76	0.86	0.0483	0.1807	16.7	78.7	4.6
3-Q-23	0.19	4.54	0.97	0.0419	0.2137	14.5	93.3	---
3-Q-24	0.20	4.49	0.79	0.0445	0.1759	15.2	76.6	8.2
3-Q-25	0.22	4.38	0.81	0.0502	0.1849	17.4	80.6	2.0

Table 22. Quantitative X-Ray Diffraction Data for High Alumina Refractory

I. Room Temperature

Specimen Number	Integrated Area of Reflection for Mullite	CaF_2	Al_2O_3	$\frac{Am}{A_{CaF_2}}$	$\frac{Aa}{A_{CaF_2}}$	Weight Per cent of Mullite	Al_2O_3	Glass
R-3-Q-26	0.21	4.57	0.84	0.0460	0.1838	15.8	80.5	3.7
R-3-Q-27	0.22	4.64	0.82	0.0474	0.1767	16.4	76.7	6.9
R-3-Q-28	0.21	4.66	0.86	0.0451	0.1845	16.0	80.4	3.6
R-3-Q-29	0.18	4.17	0.77	0.0432	0.1847	15.5	80.4	4.1
R-3-Q-30	0.24	4.83	0.89	0.0497	0.1843	17.0	80.6	2.4

J. 2800°F

Specimen Number	Integrated Area of Reflection for Mullite	CaF_2	Al_2O_3	$\frac{Am}{A_{CaF_2}}$	$\frac{Aa}{A_{CaF_2}}$	Weight Per cent of Mullite	Al_2O_3	Glass
3-Q-26	0.21	4.28	0.75	0.0491	0.1752	16.9	76.2	6.9
3-Q-27	0.20	4.26	0.77	0.0469	0.1808	16.2	78.9	4.9
3-Q-28	0.22	4.62	0.82	0.0476	0.1775	16.4	77.3	6.3
3-Q-29	0.23	4.69	0.87	0.0490	0.1855	16.9	81.0	2.1
3-Q-30	0.17	4.27	0.81	0.0398	0.1897	13.7	82.5	3.8

APPENDIX F

LATTICE PARAMETER CALCULATIONS

A sample calculation for the lattice parameters of mullite using data obtained from a room temperature specimen of mullite firebrick is shown below.

(1) The x-ray data used for the calculations is as follows:

Reflections	$2\theta CuK_{\alpha_1}$	$\underline{d}$ Value (Å)
(041)	57.48	1.6019
(401)	58.40	1.5789
(331)	60.69	1.5246
(002)	64.49	1.4436
(250)	65.47	1.4244
(440)	69.75	1.3470

For the orthorhombic system, the relation between lattice parameters and the interplanar spacing is given by the equation:

$$\frac{1}{\underline{d}^2} = \frac{\underline{h}^2}{\underline{a}^2} + \frac{\underline{k}^2}{\underline{b}^2} + \frac{\underline{l}^2}{\underline{c}^2} \qquad (6)$$

(2) The value of $\underline{c}$ is obtained from the reflection (002)

$$\underline{d} = 1.4436$$

$$\underline{c} = 2.887\underline{2}$$

(3) Calculation of $\underline{a}$ and $\underline{b}$ from $\underline{c}$ and the (041) and (401)

reflections:

Substituting the values for $\underline{d}$, $\underline{h}$, $\underline{k}$, and $\underline{l}$ in equation (6) one obtains

$$\frac{1}{(1.6019)^2} = \frac{16}{\underline{b}^2} + \frac{1}{(2.8872)^2}$$

and

$$\frac{1}{(1.5789)^2} = \frac{16}{\underline{a}^2} + \frac{1}{(2.8872)^2}$$

Solving the equations, one obtains

$$\underline{a} = 7.544$$

$$\underline{b} = 7.702$$

(4) Calculation of better-estimated $\underline{a}$ and $\underline{b}$ from the (250) and (440) reflections:

Equation (6) can be written as

$$\frac{1}{\underline{d}^2} = \frac{\underline{h}^2}{\underline{a}^2} + \frac{\underline{k}^2}{\underline{b}^2} \quad \text{if } \ell = 0$$

Then

$$\frac{1}{\underline{d}^2} = \frac{1}{\underline{a}^2}\left[\underline{h}^2 + \frac{\underline{a}^2}{\underline{b}^2} \cdot \underline{k}^2\right] = \frac{1}{\underline{b}^2}\left[\underline{k}^2 + \frac{\underline{b}^2}{\underline{a}^2} \cdot \underline{h}^2\right]$$

Substituting the values for $\underline{d}_{250}$, $\underline{d}_{440}$, and using the values of $\underline{a}^2/\underline{b}^2$ and $\underline{b}^2/\underline{a}^2$ obtained from the (041) and (401) reflections and solving the equations for $\underline{a}$ and $\underline{b}$ one obtains

$$\underline{a} = 7.535 \text{ Å} \qquad \underline{b} = 7.693 \text{ Å}$$

$$\underline{a} = 7,542 \text{ Å} \qquad \underline{b} = 7.700 \text{ Å}$$

The average values for $\underline{a}$ and $\underline{b}$ are

$$\underline{a} = 7.530 \pm 0.001 \text{ Å}$$

$$\underline{b} = 7.696 \pm 0.001 \text{ Å}$$

(5) Calculation of better estimated $\underline{c}$ using the average values of $\underline{a}$ and $\underline{b}$ and the reflection (331):

Substituting the values for $\underline{a}$ and $\underline{b}$ in equation (6) and solving for $\underline{c}$ one obtains

$$\underline{c} = 2.888$$

Hence the average value of $\underline{c}$ = 2.888 ± 0.001 Å

(6) Calculation of cell volume:

Using the values $\underline{a}$ = 7.539, $\underline{b}$ = 7.696, and $\underline{c}$ = 2.888, the cell volume is

$$C_v = \underline{a}\,\underline{b}\,\underline{c} = 167.5 \text{ Å}^3$$

A sample calculation of the lattice parameters of alumina using data obtained from a room temperature specimen of a high alumina refractory is shown below.

(1) The x-ray data used for the calculation is as follows:

Reflection	$2\theta Cu_{K_{\alpha_1}}$	$\underline{d}$ Value (Å)
(124)	66.51	1.4046
(300)	68.21	1.3737

For the hexagonal system, the relationship between lattice parameters and the interplanar spacing is given by the equation

$$\frac{1}{\underline{d}^2} = \frac{4}{3}\left[\frac{\underline{h}^2 + \underline{h}\,\underline{k} + \underline{k}^2}{\underline{a}^2}\right] + \frac{\underline{\ell}^2}{\underline{c}^2} \qquad (7)$$

(2) The value of $\underline{a}$ is obtained from the reflection (300)

$$\frac{1}{(1.3737)^2} = \frac{4}{3}\left[\frac{3^2}{\underline{a}^2}\right]$$

$$\underline{a} = 4.759 \pm 0.001 \text{ Å}$$

(3) The value of $\underline{c}$ is obtained from the (124) reflection and the value of $\underline{a}$.

$$\frac{1}{(1.4046)^2} = \frac{4}{3}\left[\frac{1^2 + 2 + 2^2}{22.6452}\right] + \frac{4^2}{\underline{c}^2}$$

$$\underline{c} = 12.991 \pm 0.001 \text{ Å}$$

(4) Calculation of the unit cell volume:

For the hexagonal system, the unit cell volume is given by:

$$C_v = 0.866\ \underline{a}^2\ \underline{c} \qquad (8)$$

Using the values of $\underline{a} = 4.759$ and $\underline{c} = 12.991$, the unit cell volume, C_v, is 256.7 Å^3.

BIBLIOGRAPHY

LITERATURE CITED

1. Hunt, E. G., and Bradley, R. S., "Description of Hot Modulus of Rupture and Hot Crushing Strength Test and Discussion of Results," Bulletin of the American Ceramic Society, 20, 267 (1941).

2. Ford, W. F., and White, J., "The Mechanical Properties of Basic Refractories at High Temperatures," Transactions of the British Ceramic Society, 56, 309 (1957).

3. Davis, W. R., and Rigby, G. R., "Basic Refractories: Variation with Temperature of Modulus of Elasticity," Transactions of the British Ceramic Society, 56, 259 (1957).

4. Wiechula, B. A., and Roberts, A. L., "The Elastic and Viscous Properties of Alumino-Silicate Refractories," Transactions of the British Ceramic Society, 51, 173 (1952).

5. Fleming, J. D., and Others, Fused Silica Manual, Engineering Experiment Station, Georgia Institute of Technology, Atlanta, Georgia (1959-64).

6. Bush, E. A., and Hummel, F. A., "High Temperature Mechanical Properties of Ceramic Materials: II, Beta-Eucryptite," Journal of the American Ceramic Society, 42, 388 (1959).

7. Bush, E. A., and Hummel, F. A., "High Temperature Mechanical Properties of Ceramic Materials: I, Magnesium Dititanate," Journal of the American Ceramic Society, 41, 189-195 (1958).

8. Davis, W. R., and Rigby, G. R., "The Measurement of Young's Modulus of Silica Refractories at High Temperatures," The Gas Council, 46th Report of the Joint Refractories Committee, 47 (1954-55).

9. Davis, W. R., and Rigby, G. R., "The Measurement of Young's Modulus of Alumina-Silica Refractories," The Gas Council, 47th Report of the Joint Refractories Committee, 40 (1955-56).

10. Miller, E. D., and Davis, B., "The Modulus of Rupture of Alumina-Silica Refractories at Elevated Temperatures," 67th Annual Meeting of the American Ceramic Society, May, 1965.

11. Folk, H. F., and Bohling, W. C., "The Transverse Strength at High Temperature of Alumina-Silica," 68th Annual Meeting of the American Ceramic Society, May, 1966.

12. Rigby, G. R., "The Origin of Mechanical Strength in Ceramic Materials," Transactions of the British Ceramic Society, 50, 75 (1951).

13. Fulrath, R. M., "Internal Stresses in Model Ceramic Systems," Journal of the American Ceramic Society, 42, 423 (1959).

14. Mattyasovszky-Zsolnay, L., "Mechanical Strength of Porcelain," Journal of the American Ceramic Society, 40, 299 (1957).

15. Roberts, A. L., "Elasticity-Temperature Relationships in Refractories," Transactions of the British Ceramic Society, 53, 724 (1954).

16. Chalkader, A. C. D., and Roberts, A. L., "Relationship between Constitution and Properties of Silica Refractories-I," Transactions of the British Ceramic Society, 56, 331 (1957).

17. Aultz, N. N., and Ueltz, H. F. G., "Sonic Analysis for Solid Bodies," Journal of the American Ceramic Society, 36, 199 (1953).

18. Gillery, F. H., and Bush, E. A., "Thermal Contraction of Beta-Eucryptite ($Li_2O \cdot Al_2O_3 \cdot 2SiO_2$) by X-Ray and Dilatometer Methods," Journal of the American Ceramic Society, 42, 175 (1959).

19. Houseman, D. H., and White, J., "Development of Bond Strength During Firing," Transactions of the British Ceramic Society, 58, 231 (1959).

20. Evans, J. H., and White, J., The British Foundryman, 51, 651 (1958).

21. Allison, E. B., Brock P., and White, J., "The Rheology of Aggregates Containing a Liquid Phase with Special Reference to the Mechanical Properties of Refractories at High Temperatures," Transactions of the British Ceramic Society, 58, 495 (1959).

22. Houseman, D. H., "The Development of Bond Strength During Firing -- A New Approach and its Technological Implications," The Refractories Journal, 33, 146 (1957).

23. Chaklader, A. C. D., Carruthers, T. G., and Roberts, A. L., "The Apparent Viscosity of Refractory Materials at High Temperatures," The Refractories Journal, 36, 292 (1960).

24. Chaklader, A. C. D., and Roberts, A. L., "Relationships between Constitution and Properties of Silica Refractories-III," Transactions of the British Ceramic Society, 57, 126 (1958).

25. Studt, P. L., and Fulrath, R. M., "Mechanical Properties and Chemical Reactivity in Mullite-Glass Systems," Journal of the American Ceramic Society, 45, 182 (1962).

26. Chaklader, A. C. D., and Roberts, A. L., "Relationship between Constitution and Properties of Silica Refractories-II," Transactions of the British Ceramic Society, 57, 115 (1958).

27. Macey, H. H., "Clay-Water Relationships and the Internal Mechanism of Drying," Transactions of the British Ceramic Society, 41, 73 (1942).

28. Weyl, W. A., and Marboe, E. C., The Constitution of Glasses, Volume II, Interscience Publishers, New York, 1962.

29. Schuller, K. H., "Reactions between Mullite and Glassy Phases in Porcelain," Transactions of the British Ceramic Society, 63, 103 (1963).

30. Majumdar, and Welch, "New Data on Synthetic Mullite," Transactions of the British Ceramic Society, 62, 603 (1963).

31. Wahl, F. M., Grim, R. E., and Graf, R. B., "Phase Transformations in Silica-Alumina Mixtures as Examined by Continuous X-Ray Diffraction," The American Mineralogist, 46, 1064 (1961).

32. Rooksby, H. P., and Partridge, J. H., "X-Ray Study of Natural and Artificial Mullites," Journal of the Society of Glass Technology, 23, 338 (1939).

33. Durvoic, S., "Isomosphism Between Sillimanite and Mullite," Journal of the American Ceramic Society, 45, 157 (1962).

34. Murthy, M. K., and Hummel, F. A., "X-Ray Study of the Solid Solution of TiO_2, Fe_2O_3, and Cr_2O_3 in Mullite ($3Al_2O_3 \cdot 2SiO_2$)," Journal of the American Ceramic Society, 43, 267 (1960).

35. Aramake, S., and Roy, R., "Revised Phase Diagram for the System Al_2O_3 - SiO_2," Journal of the American Ceramic Society, 45, 229 (1962).

36. McCreery, G. L., "Improved Mount for Powdered Specimens Used on the Geiger-Counter X-Ray Spectrometer," Journal of the American Ceramic Society, 32, 141 (1949).

37. Cullity, B. D., Elements of X-Ray Diffraction, Addison-Wesley Publishing Co., 1959, p. 389.

38. Grossman, L. N., and Fulrath, R. M., "X-Ray Strain Measurement Techniques for Ceramic Bodies," Journal of the American Ceramic Society, 44, 567 (1961).

39. Natrella, M. G., Experimental Statistics, National Bureau of Standards Handbook 91, 1963.

40. Brown, S. D., and Kistler, S. S., "Devitrification of High - SiO_2 Glasses of the System Al_2O_3 - SiO_2," Journal of the American Ceramic Society, 42, 263 (1959).